

## ARTICLE

# Neutralizing antibodies protect mice against Venezuelan equine encephalitis virus aerosol challenge

Natasha M. Kafai<sup>1,2\*</sup>, Lauren E. Williamson<sup>5,6\*</sup>, Elad Binshtein<sup>5</sup>, Soila Sukupolvi-Petty<sup>1</sup>, Christina L. Gardner<sup>8,9,10</sup>, Jaclyn Liu<sup>1</sup>, Samantha Mackin<sup>1,2</sup>, Arthur S. Kim<sup>1,2</sup>, Nurgun Kose<sup>5</sup>, Robert H. Carnahan<sup>5,7</sup>, Ana Jung<sup>2</sup>, Lindsay Droit<sup>2</sup>, Douglas S. Reed<sup>8,9</sup>, Scott A. Handley<sup>2</sup>, William B. Klimstra<sup>8,9</sup>, James E. Crowe Jr.<sup>5,6,7</sup>, and Michael S. Diamond<sup>1,2,3,4</sup>

Venezuelan equine encephalitis virus (VEEV) remains a risk for epidemic emergence or use as an aerosolized bioweapon. To develop possible countermeasures, we isolated VEEV-specific neutralizing monoclonal antibodies (mAbs) from mice and a human immunized with attenuated VEEV strains. Functional assays and epitope mapping established that potently inhibitory anti-VEEV mAbs bind distinct antigenic sites in the A or B domains of the E2 glycoprotein and block multiple steps in the viral replication cycle including attachment, fusion, and egress. A 3.2-Å cryo-electron microscopy reconstruction of VEEV virus-like particles bound by a human Fab suggests that antibody engagement of the B domain may result in cross-linking of neighboring spikes to prevent conformational requirements for viral fusion. Prophylaxis or postexposure therapy with these mAbs protected mice against lethal aerosol challenge with VEEV. Our study defines functional and structural mechanisms of mAb protection and suggests that multiple antigenic determinants on VEEV can be targeted for vaccine or antibody-based therapeutic development.

## Introduction

Venezuelan equine encephalitis virus (VEEV) is a mosquito-transmitted, enveloped, positive-stranded RNA alphavirus of the *Togaviridae* family (Strauss and Strauss, 1994; Weaver et al., 2012). VEEV is part of an antigenic complex that comprises six subtypes (I–VI). Subtype I contains the epizootic VEEV strains (subtypes IAB and IC) that can cause severe disease in equids and humans and are responsible for periodic epidemics across the Americas (Forrester et al., 2017; Zacks and Paessler, 2010). VEEV subtypes ID–IF and II–VI are enzootic strains, which circulate between rodents and *Culex* mosquitoes and typically are less pathogenic in larger mammals. Expansion of mosquito vectors raises concern for possible VEEV reemergence (Guzmán-Terán et al., 2020; León et al., 2020). In addition, VEEV is a bioterrorism threat and was weaponized previously for possible aerosol dissemination (Bronze et al., 2002; Hawley and Eitzen, 2001; Sidwell and Smea, 2003). There are no

approved human vaccines or antiviral drugs for general use against VEEV. A highly reactogenic live-attenuated vaccine (TC-83) generated through serial passage of the VEEV Trinidad Donkey (TrD) strain is available through the United States Army Special Immunizations Program for at-risk laboratory workers and military personnel (Berge et al., 1961; Edelman et al., 1979; Jahrling and Stephenson, 1984; Kinney et al., 1993; Ronca et al., 2016).

The RNA genome of VEEV is ~11.5 kb in length and encodes four nonstructural proteins, nsP1–4, and five structural proteins, capsid (C), p62 (E3 and E2), 6K, and E1, in two open reading frames (Leung et al., 2011). The mature virion includes a nucleocapsid surrounded by a lipid envelope embedded with heterodimers of the envelope glycoproteins, E2 and E1. The E2-E1 heterodimers assemble into 80 trimeric spikes on the viral surface (Voss et al., 2010; Zhang et al., 2011). The E2 protein

<sup>1</sup>Department of Medicine, Washington University School of Medicine, St. Louis, MO; <sup>2</sup>Department of Pathology and Immunology, Washington University School of Medicine, St. Louis, MO; <sup>3</sup>Department of Molecular Microbiology, Washington University School of Medicine, St. Louis, MO; <sup>4</sup>The Andrew M. and Jane M. Bursky Center for Human Immunology and Immunotherapy Programs, Washington University School of Medicine, St. Louis, MO; <sup>5</sup>Vanderbilt Vaccine Center, Vanderbilt University Medical Center, Nashville, TN; <sup>6</sup>Department of Pathology, Microbiology and Immunology, Vanderbilt University Medical Center, Nashville, TN; <sup>7</sup>Department of Pediatrics, Vanderbilt University Medical Center, Nashville, TN; <sup>8</sup>Center for Vaccine Research, University of Pittsburgh, Pittsburgh, PA; <sup>9</sup>Department of Immunology, University of Pittsburgh, Pittsburgh, PA; <sup>10</sup>United States Army Research Institute for Infectious Diseases, Fort Detrick, MD.

\*N.M. Kafai and L.E. Williamson contributed equally to this paper. Correspondence to Michael S. Diamond: [diamond@wustl.edu](mailto:diamond@wustl.edu); James E. Crowe Jr.: [james.crowe@umc.org](mailto:james.crowe@umc.org); William B. Klimstra: [klimstra@pitt.edu](mailto:klimstra@pitt.edu).

© 2022 Kafai et al. This article is distributed under the terms of an Attribution–Noncommercial–Share Alike–No Mirror Sites license for the first six months after the publication date (see <http://www.rupress.org/terms/>). After six months it is available under a Creative Commons License (Attribution–Noncommercial–Share Alike 4.0 International license, as described at <https://creativecommons.org/licenses/by-nc-sa/4.0/>).

protrudes from each spike to facilitate attachment and entry through receptor-mediated endocytosis. Low-density lipoprotein receptor class A domain-containing 3 (LDLRAD3) is a recently described entry receptor required for VEEV infection (Ma et al., 2020). E2 consists of several domains, listed here from most membrane distal to proximal on the spike: domain B (residues 173–231), N-linker (residues 1–15), domain A (residues 16–134),  $\beta$ -ribbon connector (residues 132–170 and 232–270), domain C (residues 269–341), and stem region or domain D (residues 342–367; Smith et al., 1995; Voss et al., 2010; Zhang et al., 2011). The E1 protein lies beneath E2 at the base of each trimeric spike and mediates low-pH endosomal fusion via a hydrophobic fusion loop before release of the viral nucleocapsid into the cytoplasm (Lescar et al., 2001).

The E2 protein is a target of potentially neutralizing anti-alphavirus antibodies (Burke et al., 2019; Casals et al., 1973; Fox et al., 2015; Hülseweh et al., 2014; Kim et al., 2019; Morgan et al., 1942; Williamson et al., 2020). Neutralizing anti-VEEV murine mAbs were generated in the early 1980s and used to probe the antigenic structure of alphavirus envelope glycoproteins (Roehrig et al., 1982; Roehrig and Mathews, 1985). These mAbs target sites within domains A and B of the E2 protein (Porta et al., 2014; Roehrig et al., 1982; Roehrig and Mathews, 1985). Four of the domain B mAbs, 1A3B-7, 1A4A-1, 3B2A-9, and 3B4C-4, were humanized and conferred protection in rodent and nonhuman primate models of VEEV infection (Burke et al., 2019; Goodchild et al., 2011; Hu et al., 2007; Hunt et al., 2006; O'Brien et al., 2009; Phillpotts et al., 2002). Separately, a protective human mAb, F5, derived by phage display from a VEEV TC-83-vaccinated individual, mapped to E2 domain A residues 115–119 and appeared to cross-link E2 glycoproteins within a trimeric spike for inhibition of viral infection (Hunt et al., 2011; Hunt et al., 2010; Porta et al., 2014). Although several anti-VEEV mAbs protect in animal models, their mechanisms of action and corresponding binding epitopes remain uncertain.

Here we describe the molecular basis of neutralization of murine and human mAbs targeting several E2 epitopes. These mAbs block multiple steps in the viral replication cycle including viral attachment, fusion to host membranes, and egress. Epitope mapping identified antigenically distinct sites on the VEEV E2 protein targeted by mAbs. Cryo-electron microscopy (cryo-EM) analysis of the potentially neutralizing human mAb, hVEEV-63, bound to VEEV TC-83 virus-like particles (VLPs), defined a critical binding site within domain B of the E2 protein. Anti-VEEV mAbs targeting each antigenic site showed robust protective and postexposure therapeutic efficacy in mice challenged with aerosolized VEEV, highlighting multiple targets for potential therapeutic development or vaccine immunogen design.

## Results

### Isolation of neutralizing murine and human anti-VEEV mAbs

We generated anti-VEEV mAbs from mice or a human subject immunized with live-attenuated VEEV strains. Murine mAbs were created using two separate immunization schemes (see Materials and methods). We isolated 14 murine anti-VEEV mAbs

exhibiting neutralizing activity against both Sindbis virus (SINV)-VEEV TrD and VEEV TC-83. Human anti-VEEV (hVEEV) mAbs were isolated from the B cells of peripheral blood from a healthy donor who was vaccinated with VEEV TC-83. Hybridoma supernatants from 34 human B cell clones were screened for binding to VEEV TC-83 VLPs via ELISA (Ko et al., 2019; Williamson et al., 2021). Seven mAbs were isolated, with only one (hVEEV-63) potentially blocking SINV-VEEV TrD and VEEV TC-83 infections (Fig. 1 C). All neutralizing anti-VEEV mAbs bound directly to recombinant VEEV TC-83 E2 protein by ELISA (Fig. S1 A). Anti-VEEV mAbs were subcloned and purified using affinity chromatography. Neutralizing murine mAbs were of the IgG1, IgG2b, and IgG2c subclass, and hVEEV-63 was of the IgG1 subclass (Table 1).

### Neutralizing anti-VEEV mAbs compete for binding to epitopes on the VEEV E2 glycoprotein

To classify the 15 prioritized mAbs into antigenic groups, we performed competition binding analyses via ELISA with VEEV TC-83 VLPs. An unlabeled anti-VEEV mAb was incubated with VLPs before the addition of a second, biotinylated anti-VEEV mAb. A decrease in relative binding signal of the biotinylated anti-VEEV mAb suggests competitive binding and recognition of a shared antigenic site with the unlabeled mAb. This analysis classified the mAbs into three binding groups: group I (mVEEV-8, mVEEV-10, mVEEV-19, mVEEV-36, and mVEEV-68), group II (mVEEV-1, mVEEV-59, hVEEV-63, and mVEEV-TRD15), and group III (mVEEV-57, mVEEV-71, mVEEV-TRD13, mVEEV-TRD14, and mVEEV-TRD21; Fig. 1 A). mVEEV-43 poorly bound to VLPs and was excluded from the binning classifications (ungrouped). Some anti-VEEV mAbs partially competed for binding across groups, suggesting their epitopes are near each other. For instance, mVEEV-1 in group II competed with mVEEV-71 in group III.

### Cross-reactive binding patterns of neutralizing anti-VEEV mAbs

We evaluated the panel of neutralizing mAbs for cross-reactive binding to other alphaviruses. Using flow cytometry, we incubated mAbs with Vero cells infected with chimeric SINV strains encoding the structural proteins of the Eastern (EEEV, FL93-939) or Western (WEEV, CBA87) equine encephalitis viruses (Zhang et al., 2018) and two representative arthritogenic alphaviruses, chikungunya (CHIKV, 181/25) or Mayaro virus (MAYV, BeH407; Fig. 1 B; and Fig. S1, B and C). Although the anti-VEEV mAbs bound to SINV-VEEV infected cells, they did not bind to cells infected with the closely (SINV-EEEV or -WEEV) or distantly (CHIKV or MAYV) related alphaviruses.

The VEE antigenic complex comprises multiple subtypes (epizootic subtypes IAB and IC; enzootic subtypes ID–IF and II–VI; Fig. 1 B). VEE complex subtype I viruses share ~78–99% amino acid identity in the E2 structural proteins and at least ~74% amino acid identity with the subtype II–VI viruses (Figs. S2 and S3). To assess the binding breadth of anti-VEEV mAbs, Expi293F cells were transfected with the structural genes (C-p62-6K-E1) of different alphavirus subtypes and then tested for surface binding of individual mAbs by flow cytometry (Fig.

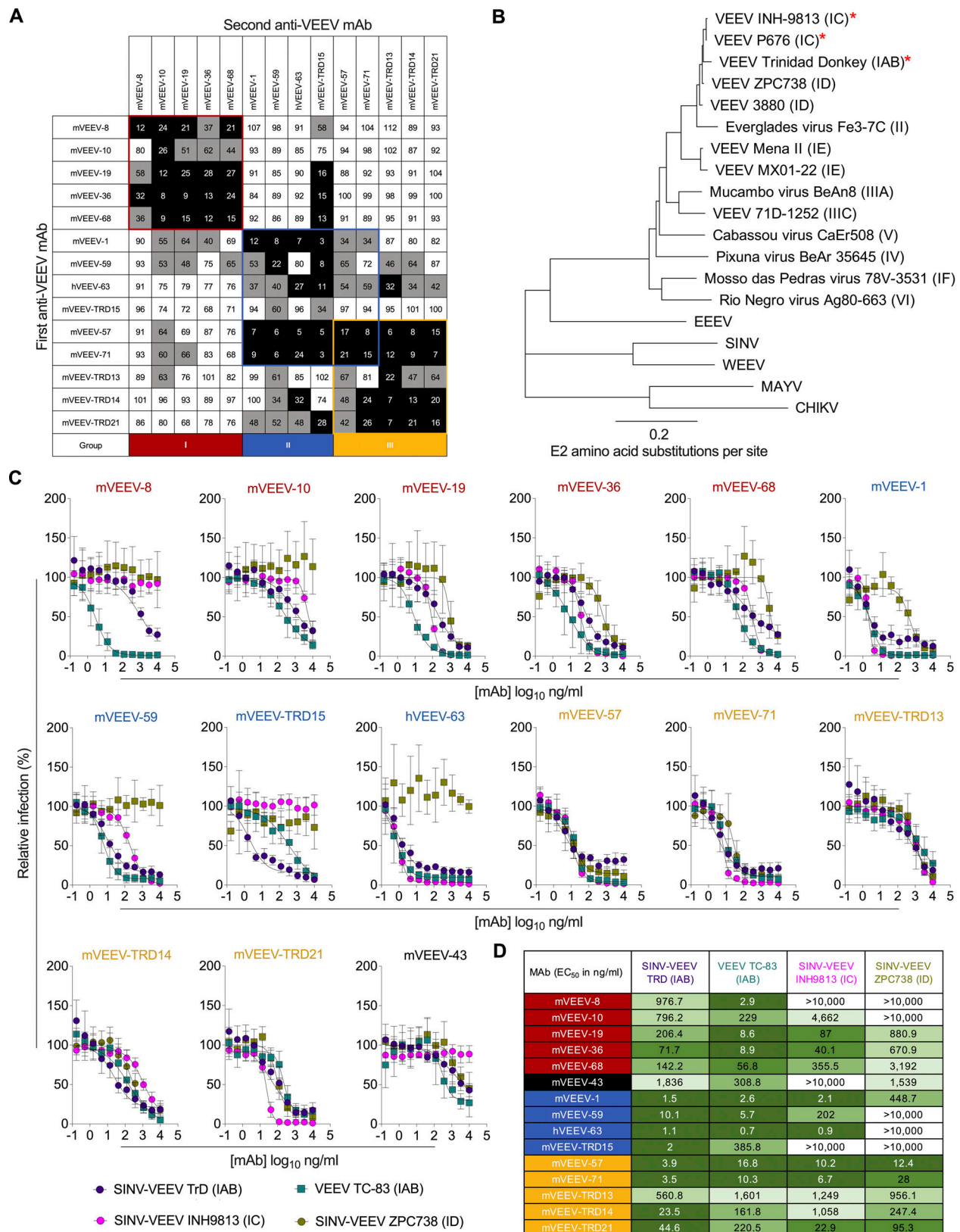


**Figure 1. Neutralizing anti-VEEV mAbs recognize distinct epitopes. (A)** Competition binding analysis of neutralizing anti-VEEV mAbs to VEEV TC-83 VLPs (subtype IAB) as determined by biolayer interferometry. The first mAb incubated with VEEV TC-83 VLPs is shown in the left column, and the second mAb is shown in the top row. Three competition binding groups were recognized by anti-VEEV mAbs (group I, red; group II, blue; and group III, yellow). mVEEV-43 poorly bound to VLPs and was excluded from the binning classifications (ungrouped, black). Loss-of-binding of the second mAb in the presence of the first mAb indicates competition (black boxes; <33% maximal binding), intermediate competition (gray boxes; 33–67% maximal binding), or no competition (white boxes;



>67% maximal binding). Competition binding groups are indicated with colored boxes. Data are representative from two experiments performed in technical duplicate. **(B)** Dendrogram showing the phylogenetic relationship of VEE subtypes and related alphaviruses used in this study. E2 amino acid sequences of VEEV INH9813 (subtype IC), VEEV P676 (IC), VEEV TrD (IAB), VEEV ZPC738 (ID), VEEV 3880 (ID), Everglades virus Fe3-7C (II), VEEV Mena II (IE), VEEV MX01-22 (IE), Mucambo virus BeAn8 (IIIA), VEEV 71D-1252 (IIIC), Cabassou virus CaEr508 (V), Pixuna virus BeAr 35645 (IV), Mosso das Pedra virus 78V-3531 (IF), Rio Negro virus Ag80-663 (VI), EEEV 76V-25343, WEEV McMillan, SINV, MAYV BeH407, and CHIKV 181/25 were aligned, and a phylogenetic tree was produced using the Tamura–Nei genetic distance model and neighborhood joining tree build method in Geneious Prime. Epizootic VEEV strains are annotated with a red star. **(C)** Anti-VEEV mAbs were assayed for neutralization of SINV-VEEV TrD (IAB, purple circles), VEEV TC-83 (IAB, teal squares), SINV-VEEV INH9813 (IC, pink circles), and SINV-VEEV ZPC738 (ID, light green circles) in Vero cells. Dose–response neutralization curves for selected mAbs against each indicated VEEV strain are shown. Data are the mean  $\pm$  SD from three experiments performed in technical duplicate. Antibodies are colored by competition groups. **(D)** Neutralization EC<sub>50</sub> values (ng/ml) from C are summarized, with more potent inhibition (lower EC<sub>50</sub> values) indicated by darker shading.

**S1 D**). The anti-VEEV mAbs displayed a range of VEE subtype specificity. As expected, all mAbs bound to cells expressing the structural proteins of the epizootic VEEV TrD or TC-83 strains. Reactivity to enzootic subtypes is of interest, as these strains can give rise to ones responsible for epizootic outbreaks (Anishchenko et al., 2006; Brault et al., 2004; Young and Johnson, 1969). The group II and III mAbs bound to fewer VEE subtypes than group I mAbs. Group III mAbs bound enzootic subtype ID (VEEV 3880) and IE (VEEV Mena II and MX01-22) structural proteins, whereas group II mAbs bound poorly or not at all. In comparison, group I mAbs bound to cells expressing the VEEV ID strain but poorly to cells expressing VEEV IE structural proteins. All group I mAbs and one group III mAb, mVEEV-71, reacted with the structural proteins of a subtype IF strain (Mosso das Pedras virus). Although the mAbs target subtype I strains that cause the majority of clinically relevant VEEV infections, a subset of our panel also bound structural proteins of subtype II (Everglades virus) and subtype IIIA (Mucambo virus) viruses, which also can cause disease in humans (Aguilar et al., 2004; Blosser and Burkett-Cadena, 2017; Calisher et al., 1980). Although no single anti-VEEV mAb bound all nine VEE antigenic complex subtypes tested, mVEEV-43 (ungrouped), mVEEV-10 (group I), and mVEEV-71 and mVEEV-TRD21 (group III) bound up to seven different strains. The mAbs generally failed to react with more distantly related VEE antigenic complex strains including those from subtypes IV (Pixuna virus), V (Cabassou virus), and VI (Rio Negro virus). This pattern of mAb reactivity with the more closely but not distantly related VEE antigenic complex subtypes likely explains the lack of binding to other alphaviruses tested (EEEV, WEEV, CHIKV, and MAYV).

#### Quantitative analysis of neutralization by anti-VEEV mAbs

We measured the inhibitory activity of the mAbs using focus reduction neutralization tests (FRNTs; Fig. 1 C and Table 1). Potent neutralization (half-maximal effective concentration [EC<sub>50</sub>] values <11 ng/ml) was observed for all group II mAbs against SINV-VEEV TrD and two mAbs in group III (mVEEV-57 and mVEEV-71). Additionally, six mAbs in groups I (mVEEV-8, mVEEV-19, and mVEEV-36) and II (mVEEV-1, mVEEV-59, and hVEEV-63) strongly neutralized VEEV TC-83, whose structural proteins are closely related to VEEV TrD. Overall, group I mAbs and the ungrouped mVEEV-43 showed weaker inhibitory activity against SINV-VEEV TrD than VEEV TC-83. Group II and III mAbs neutralized infection of both SINV-VEEV TrD and VEEV TC-83, with the exception of mAbs isolated from mice

immunized with SINV-VEEV TrD, which exhibited greater potency against the homologous virus.

To evaluate for breadth of mAb inhibitory activity, we assessed neutralization of additional SINV-VEEV strains expressing the structural genes of epizootic VEEV INH9813 (subtype IC) and enzootic VEEV ZPC738 (ID) viruses (Fig. 1 C). These viruses have a high degree of amino acid sequence identity in E2 (97.2–97.4%) compared with epizootic subtype IAB VEEV TrD (Figs. S2 and S3). Nine mAbs (mVEEV-1, mVEEV-19, mVEEV-36, mVEEV-57, mVEEV-68, mVEEV-71, mVEEV-TRD13, mVEEV-TRD14, and mVEEV-TRD21) neutralized the IAB, IC, and ID strains tested. Three mAbs (mVEEV-10, mVEEV-59, and hVEEV-63) neutralized SINV-VEEV encoding structural proteins of the epizootic (VEEV TrD [IAB] and VEEV INH9813 [IC]) but not enzootic (VEEV ZPC738 [ID]) strains. The ungrouped mAb, mVEEV-43, neutralized SINV-VEEV TrD (IAB) and SINV-VEEV ZPC738 (ID) but not SINV-VEEV INH9813 (IC). Although group II mAbs poorly neutralized the SINV-VEEV ZPC738 (ID) strain, they potently inhibited infection of SINV-VEEV TrD, expressing structural proteins of the immunizing strain. All anti-VEEV mAbs with neutralizing activity (EC<sub>50</sub> <300 ng/ml) against SINV-VEEV ZPC738 (ID) were in competition group III. Overall, our panel of mAbs inhibited the SINV-VEEV strains with structural proteins of the epizootic strains with greater potency than the enzootic strains, which is consistent with their closer evolutionary relationships to the subtype IAB viruses used for immunization (Fig. 1 B).

#### Mechanisms of virus inhibition by anti-VEEV mAbs

We first tested whether neutralizing anti-VEEV mAbs could block attachment to Vero cells. SINV-VEEV TrD was premixed with mAbs before incubation with cells at 4°C. After extensive washing to remove unbound virus, virus adsorbed to the cell surface was measured by quantitative RT-PCR (RT-qPCR; Fig. 2 A). Many of our potentially neutralizing mAbs blocked virus attachment to Vero cells, similarly to mAb 3B4C-4, which inhibits cell surface attachment (Roehrig and Mathews, 1985). Two mAbs, mVEEV-TRD14 and mVEEV-TRD21, did not block virus attachment, and one, mVEEV-TRD15, appeared to enhance attachment through an undetermined mechanism (Fig. 2 A). Given its distinct, asymmetric pattern of competition for binding with group II mAbs in Fig. 1 A, mVEEV-TRD15 binding may have unique allosteric effects that impact VEEV attachment to cells.

As LDLRAD3 is a receptor for VEEV (Ma et al., 2020), with its membrane distal domain 1 (D1) engaging several residues within the viral E2 protein (Basore et al., 2021; Ma et al., 2021; Fig. S3),



Table 1. Summary of anti-VEEV mAbs

mAb	Isotype	Group	Critical binding residue(s) <sup>a</sup>	E2 domain	Mapping strategy	Neutralizing EC <sub>50</sub> (ng/ml)			Stage inhibited	Survival (%)	
						SINV-VEEV TRD (IAB)	VEEV TC-83 (IAB)	SINV-VEEV INH9813 (IC)		Prophylaxis (-24 h)	Therapy (+24 h)
mVEEV-8	IgG <sub>2b</sub>	I	L5	N	Escape	976.7	2.9	>10,000	A <sub>NV</sub> , L, F, E	90	80
mVEEV-10	IgG <sub>2c</sub>	I	N60, K62	A	Alanine	796.2	229.0	>10,000	A <sub>NV</sub> , F, E	NT	NT
mVEEV-19	IgG <sub>2c</sub>	I	D56, N332	A/C	Alanine	206.4	8.6	87.0	A <sub>NV</sub> , L, F, E	NT	NT
mVEEV-36	IgG <sub>2c</sub>	I	D56, K62	A	Alanine	71.7	8.9	40.1	A <sub>NV</sub> , L, F, E	70	70
mVEEV-68	IgG <sub>2c</sub>	I	D56, K62, G63, R64, D94, N332	A/C	Alanine	142.2	56.8	355.5	A <sub>NV</sub> , L, F, E	100	50
mVEEV-43	IgG <sub>1</sub>	N/A	L5, F6, T49, I110, L287, P292, I311, N332	N/A/C	Alanine	1,836	308.8	>10,000	A <sub>NV</sub> , E	70	50
mVEEV-1	IgG <sub>2c</sub>	II	S182	B	Alanine	1.5	2.6	2.1	A <sub>NV</sub> , L, F	100	40
mVEEV-59	IgG <sub>2b</sub>	II	K213, F217	B	Alanine	10.1	5.7	202.0	A <sub>NV</sub> , L, F	NT	NT
hVEEV-63	IgG <sub>1</sub>	II	K213	B	Alanine	1.1	0.7	0.9	A <sub>NV</sub> , F	80	80
mVEEV-TRD15	IgG <sub>2c</sub>	II	T214	B	Alanine	2.0	385.8	>10,000	A <sub>NV</sub> , L, F, E	NT	NT
mVEEV-57	IgG <sub>2c</sub>	III	S184	B	Escape	3.9	16.8	10.2	A <sub>NV</sub> , L, F, E	80	80
mVEEV-71	IgG <sub>2b</sub>	III	S184	B	Escape	3.5	10.3	6.7	A <sub>NV</sub> , L, F, E	90	80
mVEEV-TRD13	IgG <sub>2b</sub>	III	K222	B	Alanine	560.8	1,601	1,249	A <sub>NV</sub> , E	NT	NT
mVEEV-TRD14	IgG <sub>2c</sub>	III	G203, T205	B	Escape	23.5	161.8	1,058	A <sub>NV</sub> , F, E	NT	NT
mVEEV-TRD21	IgG <sub>2c</sub>	III	T221, K222, Q225	B	Escape	44.6	220.5	22.9	L, E	NT	NT

A, E2 domain A; alanine, alanine scanning mutagenesis; A<sub>NV</sub>, attachment on NZA ΔB4galT7 cells; A<sub>NV</sub>, attachment on Vero cells; B, E2 domain B; C, E2 domain C; E, egress; escape, escape mutagenesis; F, fusion; L, LDLRAD3-D1-Fc binding; N, E2 N-linker; NT, not tested.

<sup>a</sup>Residues were defined as critical for mAb binding if a mutation caused >75% loss of binding via alanine scanning mutagenesis (or >85% for mVEEV-43 and mVEEV-68) and/or a mutation was present in >60% of an escape viral population (or >20% for mVEEV-TRD21).

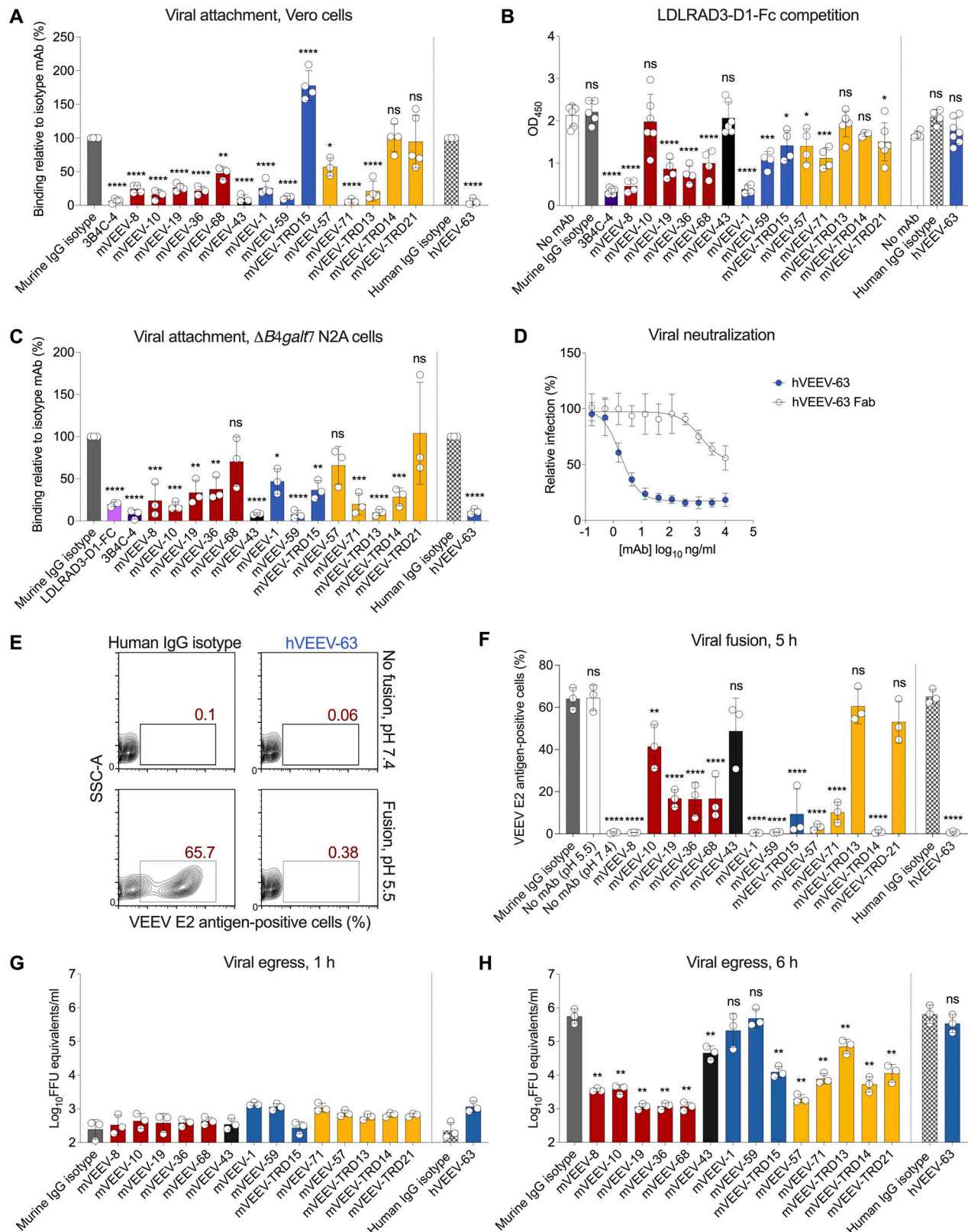


Figure 2. **Mechanisms of anti-VEEV mAb neutralization.** (A) Attachment inhibition assay on Vero cells. SIN-VEEV TrD was preincubated with anti-VEEV or isotype control mAbs (10  $\mu$ g/ml) for 1 h at 37°C before being cooled to 4°C for 1 h. Attachment reduction to Vero cells by anti-VEEV mAbs was compared to an isotype control mAb. Data represent the mean  $\pm$  SD of three to five experiments. (B) LDLRAD3-D1-Fc competition binding. ELISA plates were coated with anti-VEEV capture mAbs, murine 1A4A-1 (for murine anti-VEEV mAbs), or human DC2.112 and DC2.315 (for human anti-VEEV mAb) and then incubated with VEEV TC-83 VLPs. Subsequently, the indicated anti-VEEV mAbs were bound to VEEV TC-83 VLPs before addition and detection of LDLRAD3-D1-Fc. Data represent the mean  $\pm$  SD of four to six experiments. (C) Attachment inhibition assay on  $\Delta B4galt7$  N2A cells. SIN-VEEV TrD was preincubated with LDLRAD3-D1-Fc,

anti-VEEV, or isotype control mAbs (20  $\mu$ g/ml) for 1 h at 37°C before addition to  $\Delta B4gal7$  N2a cells at 20°C for 2 h. Data represent the mean  $\pm$  SD of three experiments performed in triplicate. **(D)** Intact mAb and Fab fragments of hVEEV-63 were assayed for neutralization of SINV-VEEV TrD in Vero cells. Dose–response neutralization curves for each are represented. Data are the mean  $\pm$  SD of three experiments performed in duplicate. **(E and F)** FFWO assay. VEEV TC-83 (MOI of 20) was adsorbed to Vero cells for 1 h at 4°C. After extensive washing to remove unbound virus, cells were incubated with 10  $\mu$ g/ml of the indicated anti-VEEV or isotype control mAbs for 1 h at 4°C. Cells were pulsed with acidic (pH 5.5) or neutral (pH 7.4) medium (negative control) at 37°C and cultured for 5 h in medium supplemented with 20 mM  $\text{NH}_4\text{Cl}$ . After fixation, cells were processed by flow cytometry for VEEV E2 antigen expression. Representative flow cytometry plots are shown (E) for a human IgG isotype control mAb and hVEEV-63 at pH 7.4 (top) or pH 5.5 (bottom) with the percentage of VEEV E2 antigen-positive cells indicated (x axis). SSC-A, side scatter area (y axis). **(F)** VEEV E2-antigen positive cells (y axis) are indicated for each mAb (x axis). Data represent the mean  $\pm$  SD of three experiments. **(G and H)** Egress blockade. Vero cells were inoculated with SINV-VEEV TrD for 2 h at 37°C and rinsed extensively. mAbs (10  $\mu$ g/ml) in medium containing 20 mM  $\text{NH}_4\text{Cl}$  were added to virus-adsorbed cells and incubated at 37°C. Supernatant was analyzed for SINV-VEEV TrD viral RNA by RT-qPCR 1 h (G) and 6 h (H) after inoculation. Values were normalized to a standard curve and represented as FFU equivalents per milliliter (y axis). Data represent the mean  $\pm$  SD of three experiments. mAbs are colored by competition groups (Fig. 1A). Murine IgG1 isotype (H77.39; Sabo et al., 2011); human IgG1 isotype (WNV hE16; Oliphant et al., 2005). Statistical significance: A, C, E, and H: one-way ANOVA with Dunnett's post-test (murine mAbs [A, E, and H], human mAbs [C]) or unpaired *t* test (human mAbs [A, E, and H]); B, one-way ANOVA with Bonferroni post-test (mAbs compared to no mAb control). \*, *P* < 0.05; \*\*, *P* < 0.01; \*\*\*, *P* < 0.001; \*\*\*\*, *P* < 0.0001.

we assessed whether our anti-VEEV mAbs could inhibit LDLRAD3 binding using a competition ELISA. Anti-VEEV mAbs were prebound to VEEV TC-83 VLPs before addition of the LDLRAD3-D1-Fc fusion protein (Fig. 2B). Most group I and II mAbs reduced LDLRAD3-D1-Fc binding. Some group III mAbs also partially competed with LDLRAD3-D1-Fc for binding. Several anti-VEEV mAbs, including mVEEV-10 (group I), hVEEV-63 (group II), mVEEV-TRD13, mVEEV-TRD14 (group III), and mVEEV-43 (ungrouped) did not block LDLRAD3-D1-Fc binding, which suggests they do not inhibit VEEV attachment to cells by directly blocking engagement of LDLRAD3.

As Vero cells lack expression of LDLRAD3 (Ma et al., 2020), they must display alternative factors for attachment and entry, possibly heparan sulfate or other glycosaminoglycans (Bernard et al., 2000; Byrnes and Griffin, 2000; Gardner et al., 2011; Silva et al., 2014). To understand how our LDLRAD3-D1-Fc competition results relate to mAb attachment inhibition on cells in which VEEV uses LDLRAD3 for entry, we repeated attachment experiments on  $\Delta B4gal7$  Neuro2a (N2a) neuronal cells (Ma et al., 2020), which express LDLRAD3 but lack heparan sulfate and other glycosaminoglycans (Fig. 2C). As expected, LDLRAD3-D1-Fc blocked SINV-VEEV attachment, whereas the murine and human isotype control mAbs did not. We observed three patterns of mAb inhibition: (1) most mAbs, including the positive control mAb 3B4C-4, blocked LDLRAD3-D1-Fc binding and also inhibited attachment to  $\Delta B4gal7$  N2a cells; (2) some mAbs failed to block LDLRAD3-D1-Fc binding by ELISA but reduced virus attachment to  $\Delta B4gal7$  N2a cells, suggesting an independent mechanism of inhibition; (3) a few mAbs partially blocked LDLRAD3-D1-Fc binding but did not inhibit attachment to  $\Delta B4gal7$  N2a cells; incomplete blockade of receptor binding may be insufficient to prevent cell attachment.

While several anti-VEEV mAbs inhibited attachment to Vero and  $\Delta B4gal7$  N2a cells and blocked LDLRAD3-D1-Fc binding, others (e.g., hVEEV-63) did not compete with LDLRAD3-D1-Fc yet still inhibited attachment to  $\Delta B4gal7$  N2a cells. One explanation for this result is that some mAbs can inhibit VEEV infection by cross-linking virus in solution (Wang et al., 2017; Zhou et al., 2020), which can prevent attachment. To begin to address this issue, we compared intact IgG and Fab fragments of hVEEV-63 for neutralization of SINV-VEEV TrD in Vero cells. Indeed, hVEEV-63 Fab fragments neutralized SINV-VEEV TrD

infection poorly ( $\text{EC}_{50}$  = 1,318 ng/ml) relative to intact hVEEV-63 IgG ( $\text{EC}_{50}$  = 1.8 ng/ml, Fig. 2D).

We next tested the mAbs for their ability to inhibit at a step after viral attachment. Viral fusogenic activity was assessed using a plasma membrane fusion-from-without (FFWO) assay (Fig. 2, E and F; Gilbert and Greenberg, 1997; Liao and Kielian, 2005; Thompson et al., 2009). In pilot studies, we found that VEEV TC-83 performed better than SINV-VEEV TrD in this assay. For this reason, VEEV TC-83 was bound to Vero cells at 4°C and subsequently incubated with anti-VEEV or isotype control mAbs. After removal of unbound virus and mAb, plasma membrane fusion was induced by a pulse of acidic medium (pH 5.5) at 37°C. Cells subsequently were incubated in medium supplemented with 20 mM  $\text{NH}_4\text{Cl}$ , which prevents de novo infection. 5 h later, and before the next cycle of infection, cells were stained for intracellular VEEV E2 antigen. Neutral-pH medium resulted in minimal expression of VEEV E2 antigen (<1% of cells), whereas a pulse of acidic-pH medium in the presence of an isotype mAb resulted in viral fusion and E2 protein expression in ~65% of cells (Fig. 2E). All group I and II mAbs tested inhibited viral fusion, as did group III mAbs mVEEV-57, mVEEV-71, and mVEEV-TRD14 (Fig. 2F).

We also evaluated whether anti-VEEV mAbs could block viral egress, presumably by inhibiting virus assembly or budding from the plasma membrane (Fig. 2, G and H). Cells were inoculated with SINV-VEEV TrD and then washed extensively to remove unbound virus. Anti-VEEV or isotype control mAbs were then added, and viral RNA in supernatants was analyzed 1 or 5 h after mAb addition. At 1 h, the level of viral RNA in supernatant was minimal, indicating that the wash steps removed the unbound inoculum (Fig. 2G). At 6 h, there was a 1,000-fold increase in viral RNA in the supernatant of isotype control mAb-treated cells, indicating secretion of newly generated virions (Fig. 2H). All group I and III mAbs blocked viral egress. mVEEV-43 and one mAb in group II, mVEEV-TRD15, also inhibited egress. However, mVEEV-1, mVEEV-59, and hVEEV-63 did not block this step. These results indicate that anti-VEEV mAbs can inhibit postentry steps in the alphavirus replication cycle in a competition group, and likely epitope-dependent, manner. Several mAbs (e.g., mVEEV-19 [group I] and mVEEV-71 [group III]) block both fusion and egress, suggesting that neutralization can occur via multiple mechanisms for a given mAb.



### Epitope mapping of anti-VEEV mAbs

We localized the binding sites of the neutralizing mAbs using alanine-scanning mutagenesis and cell surface display of wild-type and mutant VEEV structural proteins (Davidson and Doranz, 2014). HEK-293T cells were transfected with VEEV TrD p62-6K-E1 expression plasmids encoding individual alanine substitutions (or serine for alanine residues) for each residue in the E2 gene. Anti-VEEV mAbs were tested for loss of binding to transfected cells by flow cytometry. We defined critical binding residues as those with <25% mAb binding relative to a wild-type p62-6K-E1 transfected control. Cysteine residues and alanine substitutions that altered E2 conformation resulting in <70% binding by an anti-VEEV polyclonal antibody control were excluded (Fig. 3 A and Table S1). One mAb, mVEEV-8, bound relatively poorly to p62-6K-E1-transfected cells (10–30% binding to wild-type transfected cells) and was not evaluated by this method. The critical interaction residues identified using this approach were mapped onto models of VEEV E2-E1 heterodimer and trimer of dimers (Protein Data Bank [PDB] ID 7SFU; Figs. 4 and 5). Group I mAbs and the ungrouped mAb, mVEEV-43, targeted the solvent-exposed residues 56–64 at the distal tip of domain A (Fig. 4, A and B). This site is within the domain A wings (residues 52–82; strands i1–i6), which comprises two small  $\beta$ -hairpins pointing in opposite directions in the structure (Voss et al., 2010; Fig. 4). A solvent-exposed residue also was identified in the adjacent D strand (residue D94) as a target for mVEEV-68 (Fig. 4, A and B). In addition, mVEEV-43 mapped to the N-terminus of E2, termed N-linker, at residue 6 (Voss et al., 2010; Zhang et al., 2011). Residues 287, 292, 311, and 332 are in domain C, nearest the viral membrane, and were identified as interaction sites for several domain A mAbs. Mutations at these distal, buried sites may have allosteric effects that affect binding of these mAbs to domain A. Four mAbs engaged regions of domain B, with mVEEV-1 targeting residue 182 (A–B loop), and mVEEV-59, mVEEV-TRD13, and mVEEV-TRD15 mapping to residues 213 and 214 (C'–E loop) and 217 and 222 (E  $\beta$ -strand). Mapping of these residues onto the VEEV E2-E1 monomer and trimer structures revealed that several epitopes are located in patches of each domain at the top surface, center, and periphery of the E2-E1 heterodimeric spike (Fig. 4). As an unusually large number of residues across E2 domains were identified as critical for mVEEV-43 and mVEEV-68, more stringent screening criteria (<15% mAb binding relative to the wild-type) were applied to define their most critical residues, as listed in Table 1.

Using the alanine-scanning mutagenesis approach, we could not map the epitopes of mVEEV-8 and most group III mAbs (mVEEV-57, mVEEV-71, mVEEV-TRD14, or mVEEV-TRD21), as no tested mutations in E2 resulted in loss-of-binding phenotypes. To map these anti-VEEV mAbs, we selected for neutralization escape mutations. VEEV TC-83 was passaged serially in the presence of indicated anti-VEEV mAbs or an isotype control mAb until cytopathic effects were observed and VEEV TC-83 resisted neutralization (Fig. 3 B). Virus pools were subjected to next-generation sequencing to identify possible escape mutations for each mAb (Table S2). Mutations present in >60% of viral sequences and absent from the virus passaged in the presence of the isotype control mAb were introduced

individually into the VEEV TrD p62-6K-E1 plasmid to confirm loss-of-binding phenotypes (Fig. 3, C–G). Based on this analysis, mVEEV-8 (group I) targeted the N-linker at residue 5 (Table S2 and Fig. 3 C). Two mAbs, mVEEV-57 and mVEEV-71 (group III), targeted residue 184 (Table S2 and Fig. 3, D and E), which map to the A strand of domain B (Fig. 4). Of note, the escape mutation (S184G) for mVEEV-71 reduced binding by only ~50%. To corroborate this result, we substituted serine with a positively charged amino acid (S184R), which disrupted mVEEV-71 binding to a greater extent (>90% reduction). mVEEV-TRD14 (group III) targeted residues 203 and 205 (Table S2 and Fig. 3 F), in the domain B C–C' loop. The pool of escape viruses for mVEEV-TRD21 (group III) contained three different charge reversal mutations (T221K, K222E, and Q225H) in the E-strand of domain B at low frequency (Table S2 and Fig. 3 G). K222E and Q225H often were found in the same reads, suggesting these mutations are linked. While the individual substitutions only marginally affected mVEEV-TRD21 binding, combinations resulted in complete loss of binding (Fig. 3 G).

To map the human mAb hVEEV-63 (group II), we took advantage of its differential neutralization of different VEEV subtypes (Fig. 1 C and Table 1). Although hVEEV-63 neutralized SINV-VEEV strains expressing the structural proteins of epizootic IAB and IC subtypes, it did not inhibit the ID subtype tested (ZPC738). VEEV ZPC738 has a single amino acid difference at residue 213 of the E2 glycoprotein in the C'–E loop of domain B. Here a threonine substitutes the lysine in VEEV strains TrD (IAB), TC-83 (IAB), and INH9813 (IC; Fig. S3). We confirmed hVEEV-63 loss of binding to cells transfected with a plasmid encoding the K213A mutation in E2 (Fig. 3 A).

### Cryo-EM analysis of hVEEV-63 in complex with VEEV VLPs

To gain greater insight into the mode of binding and neutralization mechanisms of anti-VEEV mAbs, we selected hVEEV-63 for structural analysis due to its isolation from a vaccinated individual, potent neutralization activity through inhibition of viral fusion (Fig. 2, D and E), and protective efficacy against VEEV aerosol challenge in mice (see Figs. 6 and 7). We solved cryo-EM reconstructions of VEEV TC-83 VLPs bound with or without Fab fragments of hVEEV-63 to final resolutions of 3.2 or 4 Å, respectively (Fig. 5, A–C; Fig. S4; and Table S3). The cryo-EM reconstructions initially were at resolutions of 4.0 or 4.2 Å and were further improved through focus refinement, including mask and signal subtraction, of the asymmetric unit (Electron Microscopy Data Bank [EMDB] ID EMD-25104 and PDB ID 7SFW; Scheres, 2012). Based on the VLP-Fab complex, hVEEV-63 Fab recognized domain B of the E2 glycoprotein, which agrees with our targeted alanine mutagenesis studies with hVEEV-63 (Figs. 3 A and 5 D). hVEEV-63 Fab appears to bind at full occupancy in a radial orientation, since none of the classes showed unbound E2 protein in the asymmetric unit. Most of the asymmetric unit of the VLP-Fab complex map is near atomic resolution, which enabled visualization of the flexible loops and side chains of the structural glycoproteins (Fig. 5 D). The interface between the E2 protein and Fab involves multiple hydrogen-bonds and hydrophobic interactions between 15 residues (S184, S185, D192, K206, S208, T210, I211, N212, K213, T214, K215, Q216, F217, S218, and

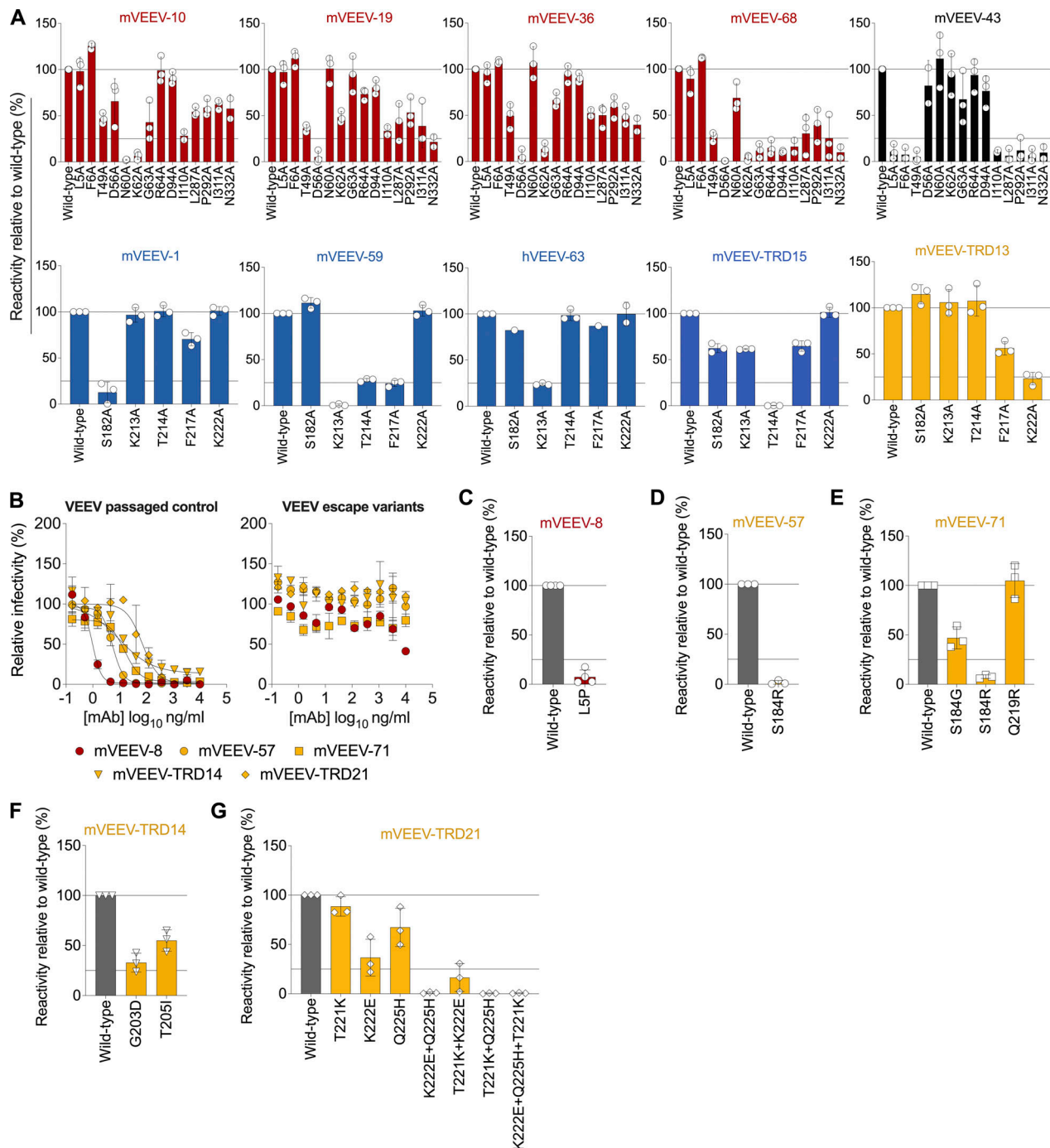


**Figure 3. Epitope mapping of anti-VEEV mAbs using alanine scanning and viral escape mutagenesis. (A)** Alanine or serine mutations were introduced at each residue of the E2 ectodomain in a plasmid encoding VEEV TrD p62-6K-E1 structural proteins. HEK-293T cells were transfected with each mutant plasmid, stained with anti-VEEV mAbs, and processed by flow cytometry. Critical binding residues for each anti-VEEV mAb are defined in Materials and methods. Data are the mean  $\pm$  SD of two to four experiments. Anti-VEEV mAb binding data spanning the entire E2 ectodomain are described in Table S1. Dotted lines indicate 25% and 100% reactivity relative to mAb binding to wild-type VEEV TrD p62-6K-E1. Data for critical residues are representative of two to three experiments. **(B)** Neutralization escape viruses were generated by serial passage of VEEV TC-83 in the presence of indicated anti-VEEV or an isotype control mAb for 6 d. Data are representative of one experiment performed in duplicate. Each anti-VEEV selection mAb was tested for neutralizing activity against a control virus pool passed in parallel with an isotype control mAb (left) and its escape virus pool (right). **(C-G)** Mutations in the escape virus pools were identified using next-generation sequencing and engineered into the plasmid encoding VEEV TrD p62-6K-E1 structural proteins for transfection of HEK-293T cells. Cells were stained with the selecting mAb and analyzed by flow cytometry. Data are the mean  $\pm$  SD from three to four independent experiments.

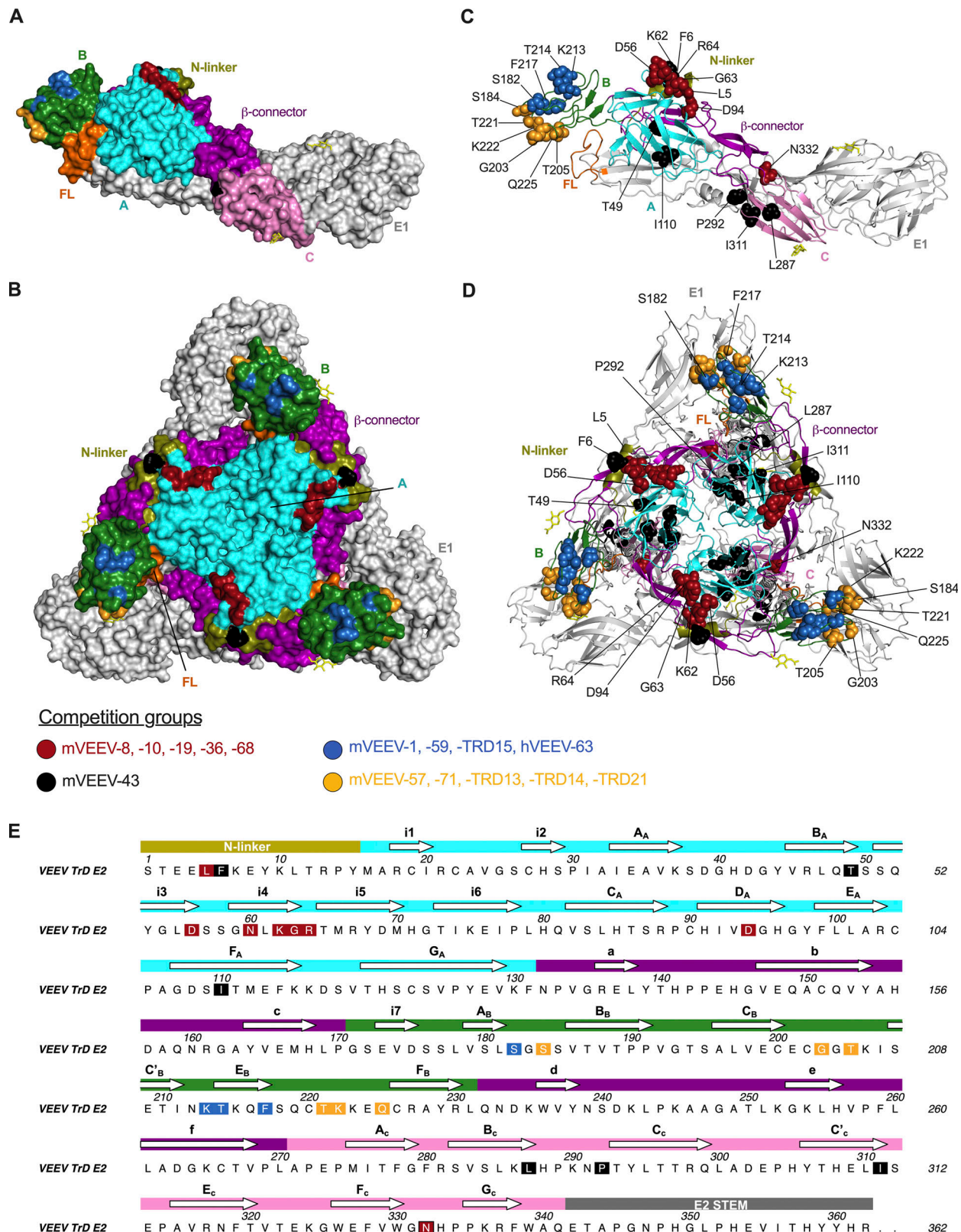


**Figure 4. Neutralizing anti-VEEV mAbs map to multiple domains of the E2 glycoprotein. (A and B)** Residues for anti-VEEV mAb engagement identified using alanine scanning and viral escape mutagenesis are diagrammed on the VEEV TC-83 E2-E1 monomer (side view; A) and trimer (top view; B). Solvent-exposed residues targeted by group I (red), group II (blue), group III (yellow), and ungrouped (black) mAbs are shown. **(C and D)** The same residues are annotated and represented on ribbon diagrams of the VEEV TC-83 E2-E1 monomer (side view; C) and trimer (top view; D). Spheres represent the van der Waals radius of an atom and are colored by competition group (group I [red], group II [blue], group III [yellow], and ungrouped [black]). Distinct E2 regions are colored accordingly: E1 (gray), E1 fusion loop (orange), E2 N-linker (olive), E2 domain A (cyan), E2 domain B (dark green), E2 domain C (pink), and E2  $\beta$ -connectors



(purple). Diagrams were constructed using PyMOL (PDB ID 7SFU). **(E)** VEEV TrD E2 amino acid sequence annotated with secondary structure components; white arrows above the sequence indicate  $\beta$  sheets. Domains are colored: E2 N-linker (olive), E2 domain A (cyan), E2 domain B (dark green), E2 domain C (pink), and E2  $\beta$ -connectors (purple). The  $\beta$ -strands in various domains are labeled with capital letters with domains A, B, or C in subscript. Lowercase letters denote strands a through f in the  $\beta$ -ribbon connector. The i1 to i7 labels are strand insertions into Ig-like domains. Critical residues for anti-VEEV mAb binding are highlighted in the sequence using their competition group colors (Fig. 1A). The black outline around the red N332 indicates this residue was identified as critical for group I mAbs (red) and for mVEEV-43 (ungrouped; black). The diagram was constructed using ALINE (Bond and Schüttelkopf, 2009).

Q219) within domain B of the E2 protein and several hVEEV-63 complementarity-determining region loop residues (heavy chain: CDHR1 [N31 and Y32], CDHR3 [N102]; light chain: CDLR1 [P28, K29, Q30, Y31, Y33] and CDLR2 [E52]; Fig. 5, E and F).

The Fab constant domain has the lowest local resolution in the EM density map, which is probably due to the flexibility and movement of this domain (Fig. 5 C). As a result, we could refine only the main chain of the Fab constant domain. Nevertheless, we observed a clear contact between neighboring Fabs of adjacent trimeric spikes along the three-fold symmetry axis, which suggests that as an IgG, hVEEV-63 may cross-link the trimeric spikes as a structural mechanism of neutralization (Fig. 5, G and H).

#### Anti-VEEV mAbs protect mice from lethal VEEV aerosol challenge

To assess the *in vivo* activity of our neutralizing anti-VEEV mAbs, we utilized a lethal challenge model of epizootic VEEV TrD in mice. 6-wk-old outbred CD-1 mice were inoculated via an aerosol route with the highly pathogenic VEEV TrD encoding a nanoluciferase reporter enzyme (Sun et al., 2014). We focused our studies on a subset of eight anti-VEEV mAbs that target distinct epitopes and demonstrate different mechanisms of neutralization. We selected four domain A-targeting mAbs: mVEEV-8, mVEEV-36, and mVEEV-68 in group I and the ungrouped mVEEV-43. Some mapped to the N-linker (mVEEV-8 and mVEEV-43) and others in the wings region (mVEEV-36 and mVEEV-68). All selected domain A mAbs block attachment, fusion, and egress, with the exception of mVEEV-43, which does not inhibit fusion. Domain B-binding mAbs in group II, mVEEV-1 and hVEEV-63, and in group III, mVEEV-57 and mVEEV-71, were chosen based on their potent neutralizing ability of SINV-VEEV TrD ( $EC_{50} < 10$  ng/ml) and ability to block fusion. Two of these mAbs, mVEEV-57 and mVEEV-71, also inhibit egress (Table 1). To assess mAb efficacy as prophylaxis, we administered a single 100- $\mu$ g (~5 mg/kg) dose of anti-VEEV mAb via i.p. injection 24 h before aerosol VEEV exposure. Mice treated with a murine or human IgG isotype control mAb developed clinical signs of disease beginning 3 or 4 d after inoculation, including ruffled fur and hunched behavior, and eventually succumbed after 5 to 10 d. Treatment with anti-VEEV mAbs targeting domains A and B resulted in 70–100% survival rates (Fig. 6, A and B). Consistent with their protective phenotype, these mAbs also reduced clinical signs of VEEV-induced disease (Fig. 6 C). Because the VEEV strain encoded for nanoluciferase, we analyzed viral replication in the brain using an *in vivo* imaging system. Representative imaging of mice 5 d after virus inoculation showed high levels of VEEV replication in isotype control mAb-treated animals (Fig. 6 D), as quantified by light intensity

per mouse (Fig. 6 E). In comparison, anti-VEEV mAbs mVEEV-8, mVEEV-68 (group I), mVEEV-1, hVEEV-63 (group II), and mVEEV-71 (group III) showed substantially reduced (~100-fold) viral infection in the brain (Fig. 6 E).

Postexposure therapy with anti-VEEV mAbs (100  $\mu$ g; ~5 mg/kg) was tested 24 h after aerosol challenge with VEEV-TrD (Fig. 7, A and B). All domain A mAbs (group I and ungrouped mAbs) tested showed therapeutic efficacy, with survival rates ranging from 50% to 70% (Fig. 7 A). With the exception of mVEEV-1, the domain B mAbs performed well as postexposure therapy, with 80% survival rates (Fig. 7 B). Clinical signs of disease (Fig. 7 C) were minimal or absent in anti-VEEV mAb-treated mice that survived compared with those that succumbed to infection. Nonetheless, for most mAbs tested, *in vivo* imaging 5 d after inoculation showed similar levels of VEEV infection compared with the isotype control mAb-treated mice (Fig. 7, D and E). Two exceptions were observed: (a) mVEEV-1 resulted in higher levels (100-fold,  $P < 0.0001$ ), and (b) treatment with hVEEV-63 resulted in decreased levels (10-fold,  $P < 0.01$ ) of VEEV replication in the brain.

## Discussion

In this study, we identified highly neutralizing anti-VEEV mAbs induced after immunization and linked their binding epitopes to mechanisms of inhibition and protective activity *in vivo*. We generated 14 neutralizing murine mAbs and one human mAb that inhibit infection at multiple steps of the viral lifecycle, including before attachment to the host cell and after entry, principally by blocking viral fusion or egress. Antibodies in our panel recognize distinct epitopes in the E2 glycoprotein in domain B (residues 182–184, 213–217, 203–205, and 221–225), the N-linker region (residues 5 and 6), and domain A (residues 49–94). Our cryo-EM reconstruction of a human Fab bound to VEEV TC-83 VLPs suggests that inhibition of viral fusion by hVEEV-63 may result from interspike cross-linking. Overall, our studies link epitopes recognized by inhibitory anti-VEEV mAbs elicited after immunization with mechanisms of neutralization and thus further define the structural and functional components that contribute to optimal protective efficacy against aerosolized VEEV infection.

Prior studies suggested that the neutralizing activity of anti-VEEV E2 mAbs in Vero cells correlated with protective efficacy in mice and nonhuman primates (Burke et al., 2019; Goodchild et al., 2011; Hu et al., 2007; Hunt et al., 2006; Phillpotts, 2006; Phillpotts et al., 2002). We similarly performed our mAb neutralization studies in Vero cells. However, the neutralizing potency of our mAbs did not directly correlate with protective efficacy in mice, suggesting that other components of antibodies

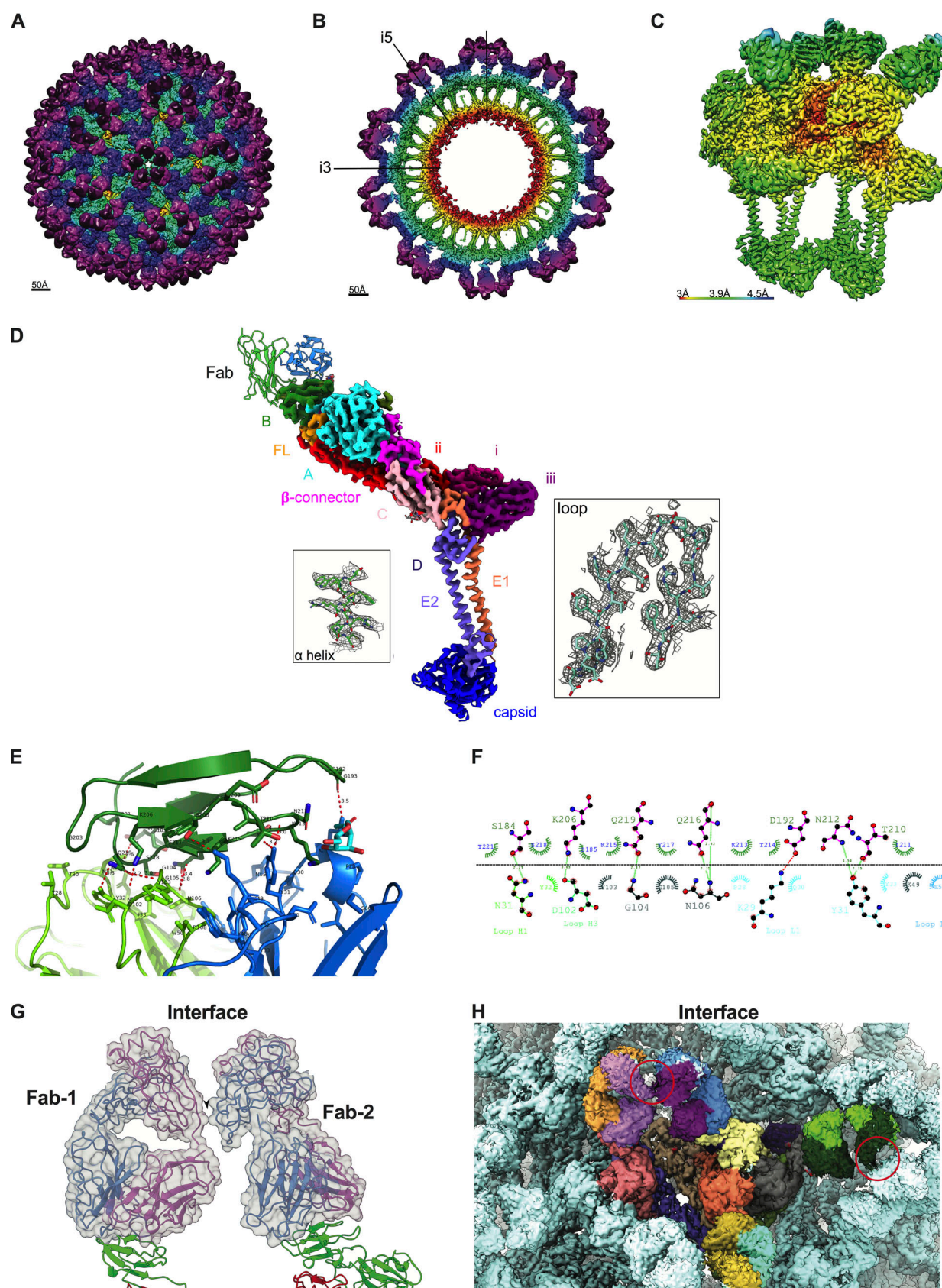


Figure 5. **Structural mechanism of hVEEV-63 binding and neutralization of VEEV.** Cryo-EM reconstruction of VEEV TC-83 VLP in complex with hVEEV-63 Fab. **(A)** Radially colored full view of the 3D reconstruction of VEEV TC-83 VLP:hVEEV-63 Fab showing Fab (pink/purple), E2 protein (blue), and E1 protein (cyan). **(B)** Radially colored central cross-section of the 3D reconstruction showing Fab (pink/purple), E2 protein (blue), E1 protein (cyan), transmembrane



domains (green), and capsid protein (yellow/red). **(C)** The asymmetric unit of the VEEV TC-83 VLP comprises four copies of E1, E2, capsid protein, and Fab. The color corresponds to local resolution as indicated by the scale bar. **(D)** EM density map of a single protomer (E1, E2, capsid, and Fab) colored by domain (E1 domains i [magenta], ii [red], iii [purple], fusion loop [yellow]; E2 domains A [cyan], B [forest green], C [light pink],  $\beta$ -connector [pink], D [violet], capsid [blue]; Fab heavy chain [light green]; Fab light chain [aqua]). The insets show the fitting of side chains in the EM map. **(E)** Side view of the interface between domain B of the VEEV TC-83 E2 protein (forest green) and hVEEV-63 Fab (heavy chain, light green; light chain, aqua). Amino acids involved in the E2-Fab interface are shown as sticks and labeled in black. Hydrogen bonds are shown by the dashed red lines. **(F)** 2D diagram of the interface between domain B of the VEEV TC-83 E2 protein (above the dashed line; forest green) and hVEEV-63 Fab (below the dashed line; heavy chain, light green; light chain, aqua). The black dashed line corresponds to the interface between E2 and the Fab. Polar bonds are colored green. Spoked arcs represent residues that make unbound contacts. **(G)** Model of two hVEEV-63 Fabs from an asymmetric unit to illustrate contacts between the Fab constant domains bound to neighboring VEEV TC-83 trimeric spikes. The distance between the closest amino acid residues of neighboring heavy and light chain Fab domains is  $\sim 3.7$  Å (black arrowhead). **(H)** One asymmetric unit of hVEEV-63 Fab bound to VEEV TC-83 VLP. Fab-Fab constant domain interactions are indicated by red circles.

(e.g., Fc effector functions) may contribute to protective phenotypes. Alternatively, antibodies can have cell type-dependent patterns of neutralization, independent of epitope-paratope interactions. For instance, neutralization activity may depend on the virus maturation state (Mukherjee et al., 2014; Vanblargan et al., 2021) or expression of cellular attachment factors or receptors in different cell lines (Chen et al., 2021).

We binned most of our neutralizing anti-VEEV mAbs into three antigenically distinct groups. Group I anti-VEEV mAbs target domain A of E2, whereas group II and III mAbs target domain B of the E2 glycoprotein. There was some overlap in competition binding between group II and group III mAbs, which can be explained by the proximity of the mapped epitopes in domain B. One mAb, mVEEV-43, bound poorly to VEEV TC-83 VLPs, which could be because it binds with low affinity to its epitope or engages a conformational or transitional epitope that is not displayed well on the VLP.

The anti-VEEV mAbs we generated did not cross-react with other alphaviruses, likely because they engage residues on E2 that are not broadly conserved among alphaviruses. The type-specificity of neutralizing anti-E2 mAbs against encephalitic alphaviruses has been described previously (Hülseweh et al., 2014; Kim et al., 2019) and contrasts with neutralizing anti-E2 mAbs targeting domain B of multiple arthritogenic alphaviruses (Earnest et al., 2019; Fox et al., 2015; Powell et al., 2020). However, many of the interaction residues for the neutralizing anti-VEEV mAbs are conserved across the VEE antigenic complex, which are 78–99% similar in their E2 amino acid sequences among subtype I strains and 74–94% similar among the subtype I and subtype II–VI strains. Identifying these broadly neutralizing anti-VEEV mAbs is of interest, since multiple VEE subtypes can infect humans (Aguilar et al., 2011; Sharma and Knollmann-Ritschel, 2019) and have potential for epidemic emergence (Guzmán-Terán et al., 2020). The breadth of mAb binding to different VEE subtypes could be explained by the conservation of interaction residues on VEEV E2. As at least one neutralizing anti-E2 domain B VEEV mAb can confer protection against subtype IAB, IC, IE, and II VEEV strains in vivo (Phillipotts, 2006), conserved epitopes may represent therapeutic targets for VEEV. Future challenge studies with other VEE complex viruses are warranted to determine the cross-protective activity of mAbs with broad VEE subtype reactivity.

Neutralizing mAbs can target different steps in the alphavirus replication cycle, and determining their mechanism of action may help establish correlates of protection in vivo (Table 1).

Prior studies with mAbs against VEEV (Mathews and Roehrig, 1982; Phillipotts, 2006; Roehrig et al., 1982; Roehrig and Mathews, 1985) suggested that neutralization may occur by blocking virus attachment to host cells and preventing fusion (Porta et al., 2014; Roehrig et al., 1988). Our most potently neutralizing anti-VEEV mAbs block both attachment and post-attachment steps. Selected mAbs from these groups showed protective efficacy as prophylaxis, with 70–100% survival rates. Analogous results of anti-E2 mAbs targeting EEEV (Kim et al., 2019; Williamson et al., 2020) and arthritogenic alphaviruses, MAYV (Earnest et al., 2019) and CHIKV (Fox et al., 2015; Jin et al., 2015), suggest that protective mAbs may share common mechanisms of neutralization at pre- and postattachment steps, with some inhibiting multiple steps in the viral replication cycle. Most mAbs in our panel inhibited at preattachment steps by blocking virion binding to host cells, including interactions with the recently identified LDLRAD3 receptor (Ma et al., 2020, 2021; Basore et al., 2021). Although many mAbs inhibited attachment to Vero and  $\Delta B4galT7$  N2a cells and blocked LDLRAD3 binding, some (e.g., hVEEV-63) that did not compete with LDLRAD3 still blocked attachment. These mAbs may inhibit VEEV attachment by a cross-linking or aggregation mechanism, as reported for other neutralizing antibodies against the related alphavirus, CHIKV (Zhou et al., 2020).

Prior mapping studies with anti-VEEV mAbs were conducted principally using neutralization escape selection. Those studies identified interaction residues on the outer surface of domain A (residues 57–59 in the domain A wings [Agapov et al., 1994]; and 115–119 in the surface exposed F-G loop [Hunt et al., 2010]) and domain B (residues 182–232 in the distal spike tip; Agapov et al., 1994; Johnson et al., 1986; Kinney et al., 1988; Kinney et al., 1989). We identified four anti-VEEV mAbs targeting solvent-exposed residues in the domain A wings region. Two domain A-binding mAbs (mVEEV-8 and mVEEV-43) also mapped to residues within the N-linker region between residues 1–6. The relatively poor neutralization of SINV-VEEV TrD compared with VEEV TC-83 by these mAbs may be due to the lysine-to-asparagine substitution at residue 7 in the N-linker region. This region becomes disordered upon furin cleavage and is conserved across VEE subtypes (Voss et al., 2010). Only one human anti-VEEV mAb, F5, targeting domain A (residues 115–119), has been tested for protective activity in vivo (Hunt et al., 2011), and cryo-EM analyses suggest that targeting domain A at this site cross-links E2 monomers within a spike to inhibit cellular attachment (Porta et al., 2014). Indeed, residues 116, 118, and 119 in domain A



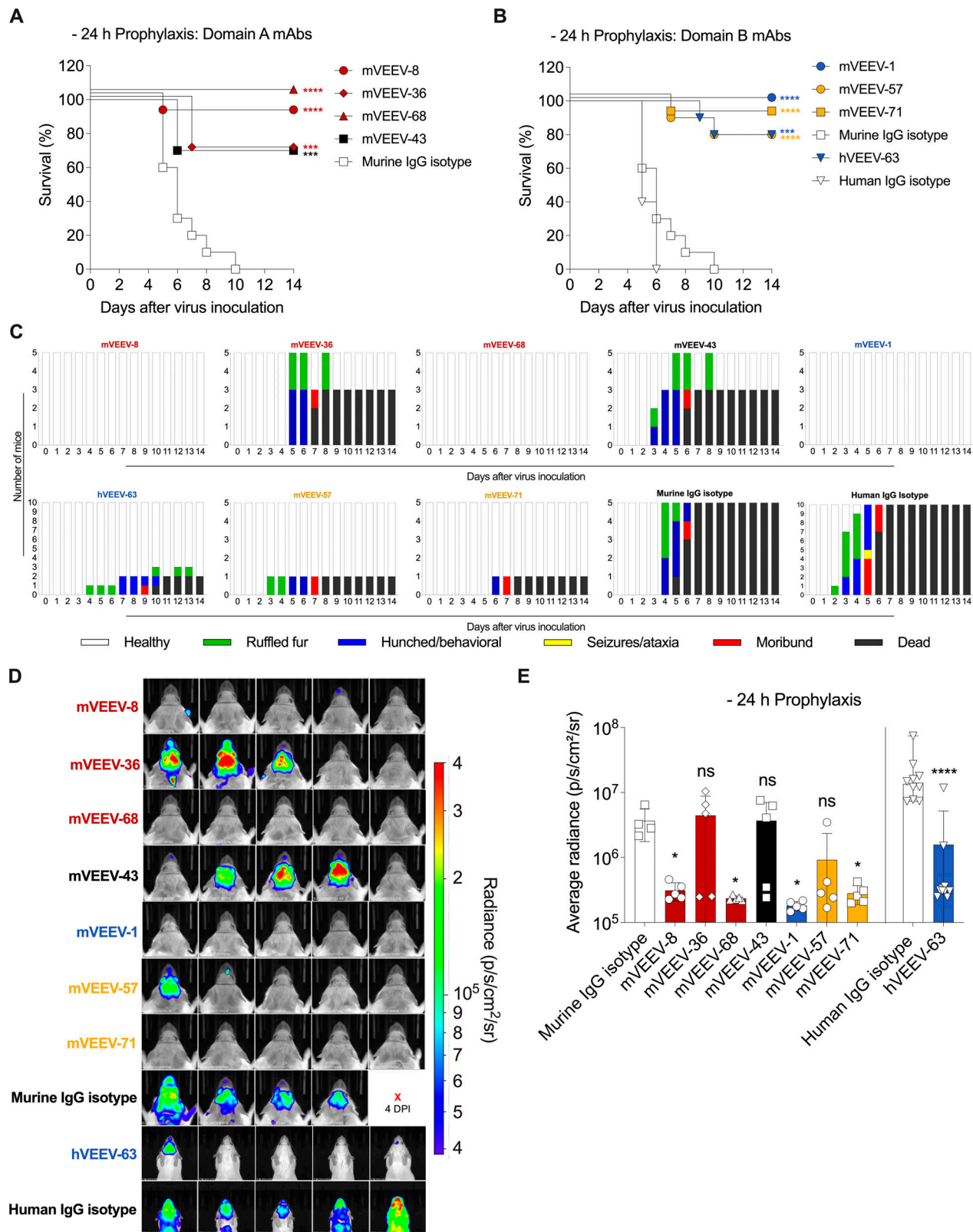


**Figure 6. Anti-VEEV mAbs protect as prophylaxis against lethal aerosol VEEV TrD challenge. (A–E)** 6-wk-old female CD-1 mice were passively administered 100  $\mu$ g of selected anti-VEEV mAbs via i.p. injection 24 h (A–E) before (– 24 h) aerosol challenge with a target dose of 50 PFU of VEEV TrD V3000 expressing a nanoluciferase enzyme (nLuc). **(A and B)** Survival data over 14 d for mice treated with domain A (group I [red], ungrouped [black]; A) or domain B (group II [blue], group III [yellow]; B) anti-VEEV mAbs are from two experiments (anti-VEEV mAbs,  $n = 10$ ; murine IgG1 isotype [H77.39],  $n = 20$ ; human IgG1 isotype [WNV hE16],  $n = 10$ ). **(C)** Clinical disease was scored daily for each mouse over 14 d and color-coded as healthy (white), ruffled fur/squinting (green), hunched/behavioral (blue), seizures/ataxia (yellow), moribund (red), and dead (black). **(D and E)** 5 d after inoculation, viral infection in brains was assessed

using an in vivo imaging system and is represented as a heatmap (D) and quantified as average radiance per mouse imaged ( $\text{p/s/cm}^2/\text{sr}$ , photons/second/centimeter<sup>2</sup>/selected region, y axis; E). The red "x" in the murine IgG isotype row in D represents one mouse death before imaging. DPI, days postinoculation. In C–E,  $n = 5$  mice per treatment group are represented for murine mAbs and  $n = 10$ , for human mAbs. Statistical significance: A and B, log-rank test with Bonferroni post-test (compared with the respective isotype control); E, one-way ANOVA (murine mAbs) or unpaired  $t$  test (human mAbs). \*,  $P < 0.05$ ; \*\*,  $P < 0.01$ ; \*\*\*,  $P < 0.001$ ; \*\*\*\*,  $P < 0.0001$ .

of E2 are contact sites for the VEEV receptor LDLRAD3 (annotated in Fig. S3; Basore et al., 2021; Ma et al., 2021). All of our domain A-targeting mAbs inhibited attachment to Vero cells, and many competed with LDLRAD3 for binding to VEEV and blocked attachment to LDLRAD3-expressing  $\Delta B4galt7$  N2a cells. These domain A mAbs map directly to LDLRAD3 contact sites at E2 residues 5, 63, 64, and 94 or proximally (residues 56–62), suggesting they can interfere with receptor binding to neutralize VEEV.

We classified nine domain B-binding anti-VEEV mAbs into two overlapping epitopes (groups II and III). With the exception of mVEEV-TRD21, all domain B mAbs demonstrated some pre-attachment inhibition activity on either Vero or  $\Delta B4galt7$  N2a cells. Murine domain B mAbs in group II block binding to LDLRAD3 and attachment to N2a cells expressing LDLRAD3. Moreover, with the exception of group III mAbs mVEEV-TRD13 and mVEEV-TRD21, domain B-targeting mAbs also block viral fusion, possibly by stabilizing E2 and preventing exposure of the E1 fusion loop. The group III mAbs generally all show the ability to block VEEV egress from cells.

We isolated one potentially neutralizing anti-VEEV human mAb, hVEEV-63, from a small panel of human mAbs. Although more analysis is needed to determine the neutralizing B cell frequency after VEEV TC-83 immunization, the low efficiency of isolation (one of 34 human B cell clones) suggests that immunization may yield a low neutralizing immune response against VEEV. hVEEV-63 blocks attachment in Vero cells, inhibits viral fusion, and was highly protective in mice. Because attachment can be cell type-dependent, but membrane fusion is required for alphavirus entry, we pursued the structural basis of inhibition by the fusion-inhibiting mAb hVEEV-63. Cryo-EM reconstructions showed that hVEEV-63 interacts with a surface-exposed epitope (residues 184–219) in domain B of E2 on the distal tip of the heterodimeric spike. hVEEV-63 may prevent fusion by stabilizing the E2 protein through the cross-linking of neighboring spikes. Cryo-EM analysis of a protective murine anti-VEEV mAb (3B4C-4), which also blocks VEEV attachment in Vero cells (Roehrig et al., 1988), shows an overlapping domain B epitope region (residues 177–223; Porta et al., 2014). In contrast to hVEEV-63, 3B4C-4 inhibits binding of LDLRAD3. Thus, neutralizing and protective mAbs targeting domain B can share some, but not all, structural and functional mechanisms of inhibition. Overall, the E2 domain B serves as a target for neutralizing and protective anti-VEEV mAbs (Hunt et al., 2010; Weger-Lucarelli et al., 2015) in mice and humans.

VEEV TrD is a Select Agent in part because of its potential for aerosolization and use as a biowarfare agent. To model this exposure to VEEV, aerosol challenge has been performed in mice and nonhuman primates (Burke et al., 2019; Gardner et al., 2017; Rusnak et al., 2018). We tested eight neutralizing mAbs targeting

domains A or B with inhibitory activity against viral fusion, egress, or both. When given 24 h before or after aerosol challenge, anti-VEEV mAbs conferred protection, with many providing close to 100% survival rates without weight loss or clinical signs of disease. Nonetheless, aerosol challenge poses a stringent challenge for systemically administered antibody therapies, as the blood-brain barrier limits efficient crossing into the brain parenchyma. Indeed, postexposure mAb therapy in the context of aerosolized EEEV showed limited efficacy (Kim et al., 2019; Williamson et al., 2020). Fc effector functions also may contribute to optimal mAb efficacy against VEEV, as we recently observed with cross-reactive anti-E1 antibodies (Kim et al., 2021). Several of our anti-VEEV mAbs performed comparably well as postexposure therapy, although the efficacy of two domain A-targeting mAbs, mVEEV-43 and mVEEV-68, decreased slightly. The success of mAb treatment after aerosol exposure typically requires early administration (e.g., within 72 h) before extensive viral replication in the central nervous system (Phillpotts et al., 2002). Further optimization of our mAbs is warranted to extend this window of therapeutic efficacy.

In summary, our study enhances an understanding of the VEEV E2 epitopes targeted by neutralizing and protective anti-VEEV mAbs and defines their functional and structural mAb properties. This work provides insight into the protective epitopes targeted by anti-VEEV mAbs, which can inform future vaccine and immunotherapy design against VEEV and possibly, related encephalitic alphaviruses.

## Materials and methods

### Human subject information

For isolation of hVEEV-63, peripheral blood was collected from an individual with a history of previous immunization with VEEV TC-83 after written informed consent. Peripheral blood mononuclear cells were isolated by density gradient purification and cryopreserved in liquid nitrogen until use. The Institutional Review Board at Vanderbilt University Medical Center approved the protocols for the recruitment and collection of blood samples used in this study.

### Cells

Cell lines were maintained at 37°C in the presence of 5% CO<sub>2</sub>. Vero (American Type Culture Collection [ATCC] CCL-81), HEK293T (ATCC CRL-3216), BHK-21 (ATCC CCL-10), or  $\Delta B4galt7$  N2a (Ma et al., 2020) cells were passaged in growth medium Dulbecco's Modified Eagle Medium (DMEM [Invitrogen] supplemented with 5% [Vero and BHK-21] or 10% [HEK293T and  $\Delta B4galt7$  N2a] heat-inactivated FBS [Omega Scientific], 100 U/ml penicillin, 100 U/ml streptomycin, and 10 mM Hepes

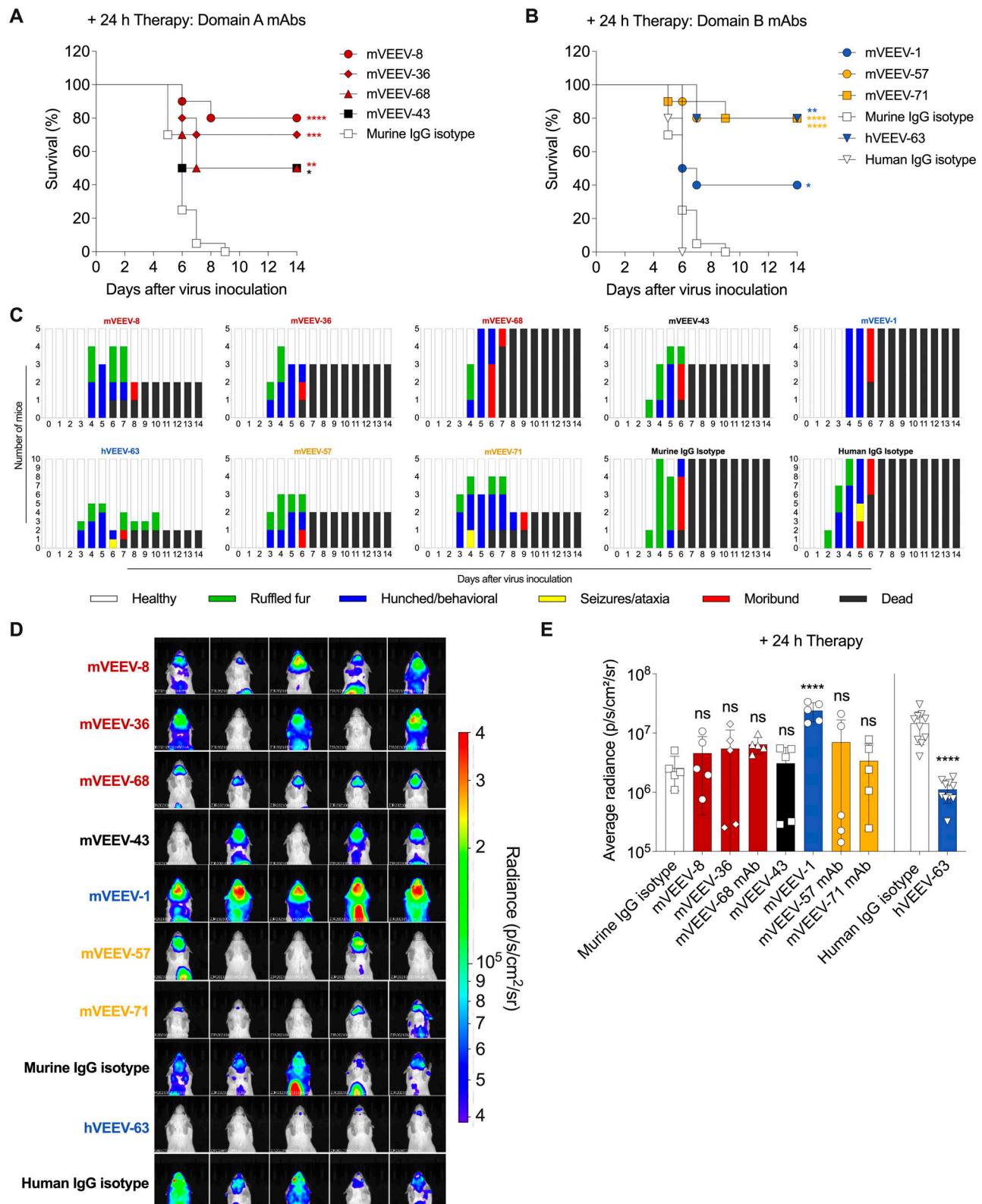


**Figure 7. Therapeutic anti-VEEV mAbs protect against lethal aerosol VEEV TrD challenge.** 6-wk-old female CD-1 mice were passively administered 100  $\mu$ g of selected anti-VEEV mAbs via i.p. injection 24 h after aerosol challenge with a target dose of 50 PFU of VEEV TrD V3000 expressing nLuc. (**A and B**) Survival data over 14 d for mice treated with domain A (group I [red], ungrouped [black]; A) or domain B (group II [blue], group III [yellow]; B) anti-VEEV mAbs are from two experiments (anti-VEEV mAbs,  $n = 10$ ; murine IgG1 isotype [H77.39],  $n = 20$ ; human IgG1 isotype [WNV hE16],  $n = 10$ ). (**C**) Clinical disease was scored daily for 14 d and color-coded as healthy (white), ruffled fur/squinting (green), hunched/behavioral (blue), seizures/ataxia (yellow), moribund (red), and dead (black). (**D and E**) 5 d after inoculation, viral infection in brains was assessed using an in vivo imaging system and is represented as a heatmap (**D**) and quantified as average radiance per mouse imaged ( $p/s/cm^2/sr$ , photons/second/centimeter<sup>2</sup>/selected region, y axis; **E**). In C–E,  $n = 5$  mice per treatment group.



are represented for murine mAbs and  $n = 10$ , for human mAbs. Statistical significance: A and B, log-rank test with Bonferroni post-test (compared with the respective isotype control); E, one-way ANOVA (murine mAbs) or Mann-Whitney test (human mAb). \*,  $P < 0.05$ ; \*\*,  $P < 0.01$ ; \*\*\*,  $P < 0.001$ ; \*\*\*\*,  $P < 0.0001$ .

[Invitrogen]). Gibco Expi293F (Thermo Fisher Scientific) cells were maintained at 37°C in Expi293 Expression Medium. Expi293F cells were authenticated by the ATCC cell line authentication service using short tandem repeat analysis. Hybridoma cell lines were grown in Iscove's Modified Dulbecco's Medium (Thermo Fisher Scientific) supplemented with 20% FBS (Hyclone), 1 mM sodium pyruvate, 100 U/ml penicillin, and 100 U/ml streptomycin (Invitrogen). HMMA 2.5, B95.8, and ExpiCHO cell lines were maintained as previously described (Williamson et al., 2020, 2021). All cell lines were confirmed as mycoplasma negative using Washington University Induced Pluripotent Stem Cell Core Facility services or using a universal mycoplasma detection kit (ATCC 30-1012K).

### Plasmids

VEEV Trinidad donkey (TrD) and TC-83 (subtype IAB, GenBank accession nos. AAC19322 and AAB02517), VEEV P676 (IC, no. AAK66990), VEEV 3880 (ID, no. AAC19325), VEEV Mena II and MX01-22 (IE, nos. AAD14553 and AAW30006), Mosso das Pedras virus 78V-3531 (IF, no. AAD14563), Everglades virus Fe3-7C (II, no. AAD14551), Mucambo virus BeAn 8 (IIIA, no. AAD14555), VEEV 71D-1252 (IIIC, no. AAD14559), Pixuna virus BeAr 35645 (IV, no. AAD14561), Cabassou virus CaAr 508 (V, no. AAD14567), Rio Negro virus Ag80-663 (VI, no. AAD14565), WEEV McMillan (no. ACT75276), or CHIKV 181/25 (no. AAA53256) structural protein genes (capsid-p62-6K-E1) were codon optimized, synthesized, and cloned into the mammalian expression vectors pcDNA3.1(+), pTwist CMV BetaGlobin, or pTwist CMV BetaGlobin WPRE Neo for expression of the different alphavirus structural proteins. All plasmids were verified by sequencing.

### Viruses

The following alphaviruses were obtained from the World Reference Center for Emerging Viruses (University of Texas Medical Branch, Galveston, TX, gift of K. Plante and S. Weaver): VEEV TC-83, CHIKV 181/25, and MAYV BeH307. Replication-competent SINV chimeric viruses SINV-VEEV (strains TrD, INH9813, and ZPC738), SINV-EEEV (FL93-939), and SINV-WEEV (CBA87) were generated by replacing the SINV-TR339 structural genes with VEEV, EEEV, or WEEV structural genes under the control of the subgenomic promoter in the SINV TR339 cDNA clone (Anishchenko et al., 2004; Gardner et al., 2017; Paessler et al., 2003). Viruses were produced by plasmid linearization, in vitro transcription with SP6 or T7 DNA-dependent RNA polymerase (mMESSAGE mMACHINE SP6 or T7 transcription kit; Invitrogen), and electroporation into BHK-21 cells. After 24–36 h, supernatant was collected and stored as a passage 0 (P0) stock at –80°C. High-titer P1 stocks were generated by inoculating Vero cells or BHK-21 cells at a multiplicity of infection (MOI) of 0.1 in infection media (DMEM [Invitrogen], 2% FBS [Omega Scientific], 100 U/ml penicillin, 100 U/ml streptomycin, and 10 mM Hepes [Invitrogen]). After incubation at 37°C in 5% CO<sub>2</sub> for 48 h, supernatants were passed through a

0.2-μm-pore-size filter and stored at –80°C. All virus titers were determined by focus-forming assay in Vero cells. The cDNA clones of VEEV TrD and nanoluciferase-expressing VEEV TrD have been described previously (Sun et al., 2014). All work with select agent VEEV TrD were performed in an ABSL3+ facility at the University of Pittsburgh in accordance with approved biosafety protocols.

### Mice

Wild-type C57BL/6J and CD-1 mice were purchased from The Jackson Laboratory and Charles River Laboratories, respectively. Mice were housed in a pathogen-free animal facility at Washington University or at the University of Pittsburgh. Animal studies were carried out in accordance with the recommendations in the Guide for the Care and Use of Laboratory Animals of the National Institutes of Health. The protocols were approved by the Institutional Animal Care and Use Committee at the Washington University School of Medicine (assurance number A3381-01) or University of Pittsburgh (assurance number D16-00118). Virus inoculations were performed under anesthesia that was induced and maintained with ketamine hydrochloride and xylazine. All efforts were made to minimize animal suffering.

### Generation of anti-VEEV mouse mAbs

8-wk-old wild-type female C57BL/6J mice were inoculated subcutaneously with 10<sup>5</sup> focus-forming units (FFU) of the live-attenuated VEEV TC-83 strain or an attenuated chimeric strain, SINV-VEEV TrD. 1 mo later and 3 d before sacrifice, mice were boosted with 10<sup>5</sup> FFU of the homologous virus. Spleens were harvested and fused with P3X63 Ag.8.6.5.3 mouse myeloma cells as described previously (Kim et al., 2019; Vanblargan et al., 2021). Hybridomas producing antibodies that bound to recombinant VEEV TrD E2 by ELISA and/or SINV-VEEV TrD-infected cells by flow cytometry were cloned by limiting dilution. Undiluted hybridoma supernatants were screened for neutralization of SINV-VEEV TRD using single-endpoint assay. mAbs were isotyped and purified by protein A affinity columns using a commercial vendor (Bio X Cell).

### Human mAb generation

Previously cryopreserved peripheral blood mononuclear cells (4–8.6 × 10<sup>6</sup> cells) were thawed rapidly and transformed with EBV, as previously described (Smith and Crowe, 2015; Williamson et al., 2020). Cells from wells containing reactive supernatants were fused with the nonsecreting myeloma cell line HMMA 2.5, using an electrofusion protocol as previously described (Smith and Crowe, 2015; Yu et al., 2008). Fused hybridomas were selected by plating in hypoxanthine/aminopterin/thymidine (HAT) medium (ClonaCell-HY Medium A, ClonaCell-HY Medium E [Stem Cell Technologies], 50× HAT medium supplement [Sigma-Aldrich], and ouabain octahydrate [Sigma-Aldrich]) at 50 μl/well in 384-well plates. The plates

were incubated for a total of 14–21 d at 37°C in a humidified atmosphere of 7% CO<sub>2</sub> before screening by ELISA. Wells containing reactive hybridomas were cloned by single-cell FACS. These hybridoma clones were expanded in ClonaCell-HY Medium E (Stem Cell Technologies) serially into 48-well plates, 12-well plates, and T-75 cm<sup>2</sup> flasks, respectively. Hybridoma clones were expanded further into T-225 cm<sup>2</sup> flasks or G-Rex devices (Wilson Wolf) in serum-free medium (Hybridoma SFM). Supernatants were harvested after ~21 d or in sets of 3–5 d, respectively, through a 0.2-μm-pore-size filter. Antibodies were purified from the filtrate using HiTrap MabSelectSure columns on an ÄKTA Pure 25M chromatography system. Antibodies were concentrated using 50K MWCO Amicon Ultra Centrifugal Filter Units followed by desalting and buffer exchange with 7K MWCO Zebra desalting columns.

### Recombinant VEEV TC-83 E2 protein production and binding ELISA

For production of VEEV TC-83 E2 ectodomain, residues 1–341 were cloned into the pET-21a *Escherichia coli* expression vector and transformed into BL21(DE3) chemically competent cells (Thermo Fisher Scientific). Cells were grown at 37°C in lysogeny broth to an OD<sub>600</sub> of 0.9 and then induced with 1 mM isopropyl-β-D-thiogalactopyranoside for 4 h. Bacteria were collected, resuspended in 50 mM Tris-HCl, 1 mM EDTA, 0.01% Na<sub>3</sub>N, 1 mM dithiothreitol, and 25% sucrose (TENDS buffer), and lysed in 50 mM Tris-HCl, 1 mM EDTA, 0.01% Na<sub>3</sub>N, 1 mM dithiothreitol, 200 mM sodium chloride, 1% sodium deoxycholate, and 1% Triton X-100. Inclusion bodies were obtained after centrifugation (6,000 g for 30 min) and then washed in TENDS buffer supplemented with 100 mM NaCl and 0.5% Triton X-100. After a final wash in the same buffer without 0.5% Triton X-100, ~200 mg of inclusion bodies were denatured in 100 mM Tris-HCl, 6 M guanidinium chloride, and 20 mM β-mercaptoethanol for 1 h. Solubilized protein was refolded overnight at 4°C into a buffer containing 400 mM L-arginine, 100 mM Tris-HCl, 5 mM reduced glutathione, 0.5 mM oxidized glutathione, 10 mM EDTA, and 200 mM phenylmethylsulfonyl fluoride. Refolded protein was concentrated using a 10-kD molecular weight cutoff stirred cell concentrator (EMD Millipore) purified by HiLoad 16/600 Superdex 75 pg size exclusion chromatography (GE Healthcare) and flash frozen using liquid nitrogen for storage at –80°C. To assess for binding to recombinant VEEV TC-83 E2, Nunc MaxiSorp plates (Thermo Fisher Scientific) were coated with 2 μg/ml of recombinant VEEV TC-83 E2 in 100 μl of coating buffer (0.1 M Na<sub>2</sub>CO<sub>3</sub> and 0.02% Na<sub>3</sub>N, pH 9.6) and incubated overnight at 4°C. Plates were washed four times with Dulbecco's PBS (D-PBS, Thermo Fisher Scientific) and incubated with 150 μl of blocking buffer (D-PBS and 4% BSA) for 1 h at room temperature. Anti-VEEV mAbs were diluted to 10 μg/ml in D-PBS containing 2% BSA and added (100 μl/well) to plates for 1 h at room temperature. Plates were washed four times with D-PBS and incubated with 100 μl/well of 1:5,000 HRP-conjugated goat anti-mouse IgG (H + L; Jackson ImmunoResearch) for detection of murine anti-VEEV mAbs and anti-human IgG (H + L; Jackson ImmunoResearch) for detection of the human anti-VEEV mAb. Plates were washed four times with D-PBS and then incubated

with 100 μl of 3,3',5,5'-tetramethylbenzidine substrate (Thermo Fisher Scientific) for 3 min at room temperature before quenching by addition of 50 μl of 2 N H<sub>2</sub>SO<sub>4</sub>. Absorbance was read at OD 450 nm with a TriStar Microplate Reader (Berthold Technologies).

### LDLRAD3-D1-Fc recombinant protein production

LDLRAD3-D1-Fc was produced using Expi293F cells, as described (Ma et al., 2020). Briefly, codon-optimized vectors encoding the LDLRAD3-D1-Fc (human IgG1 or murine IgG2b) proteins were cotransfected with receptor-associated protein, an LDL-receptor family protein chaperone. Protein was purified from supernatant using protein A Sepharose 4B (Thermo Fisher Scientific) and dialyzed into D-PBS with 1 mM CaCl<sub>2</sub> and EDTA-free protease inhibitors (Roche). Purity was confirmed by SDS-PAGE, and protein was stored at 4°C for subsequent use.

### Human hybridoma ELISA screen

VEEV TC-83 VLPs generously provided by John Mascola (National Institutes of Health Vaccine Research Center; Ko et al., 2019) and recombinant VEEV TrD E2 glycoprotein (DAGA-268; Creative Diagnostics) were diluted to 2 μg/ml in D-PBS to coat 384-well ELISA plates (Thermo Fisher Scientific) at 25 μl/well and incubated at 4°C overnight. The plates were aspirated and blocked for 1 h at room temperature with 25 μl/well of blocking solution (2% nonfat dry milk [Blotting Grade Blocker; Bio-Rad] and 2% goat serum [Gibco] in D-PBS with 0.05% Tween-20 [D-PBS-T; Cell Signaling Technology]). After blocking, the plates were washed three times with D-PBS-T, and a volume of 10–25 μl/well of supernatant from each well containing EBV-transformed B cells or hybridoma cell lines was added. Plates were incubated for 2 h at room temperature or overnight at 4°C. Plates then were washed three times with D-PBS-T, and a suspension of secondary Abs (goat anti-human IgG Fc gamma fragment-specific alkaline phosphatase [AP]-conjugated [Meridian Life Science]; and goat anti-human IgA-AP-conjugated [Southern Biotech]) at a 1:4,000 dilution in 1% blocking solution (1% nonfat dry milk and 1% goat serum) was added at 25 μl/well for 1 h at room temperature. AP substrate solution (phosphatase substrate tablets [Sigma-Aldrich] in AP substrate buffer [1 M Tris aminomethane], and 30 mM MgCl<sub>2</sub> [Sigma-Aldrich]) was added at 25 μl/well after plate washing four times with D-PBS-T. Plates were incubated at room temperature in the dark for 2 h and then read at an optical density of 405 nm with a Biotek plate reader.

### VEEV TC-83 VLP competition binding analysis

VEEV TC-83 VLPs were diluted to 2 μg/ml in D-PBS to coat 384-well plates (Thermo Fisher Scientific) and incubated at 4°C overnight. The plates were aspirated and blocked for 1 h at room temperature with blocking solution (2% nonfat dry milk and 2% goat serum in D-PBS-T). After blocking, the plates then were washed three times with D-PBS-T, and the first Ab (10 μg/ml) in blocking solution (1% non-fat dry milk and 1% goat serum in D-PBS-T) was added at 20 μl/well for 1 h at room temperature. The biotinylated second Ab (2.5 μg/ml; final concentration of 0.5 μg/ml) was added in blocking solution (1% non-fat dry milk and

1% goat serum in D-PBS-T) at 5  $\mu$ l/well for 1 h at room temperature. The plates then were washed three times with D-PBS-T and incubated with a solution of secondary Abs (mouse anti-biotin-HRP [Southern Biotech]) diluted 1:4,000 in blocking solution (1% non-fat dry milk and 1% goat serum in D-PBS-T) for 1 h at room temperature. The plates were washed four times with D-PBS-T followed by addition of One-step Ultra-TMB ELISA substrate solution (Thermo Fisher Scientific). The reaction was stopped with 1 N HCl (Thermo Fisher Scientific) and then read at an optical density of 450 nm with a Biotek plate reader. Percentage binding of each Ab was normalized to optical density value for binding in the presence of the negative control human mAb, rDENV-2D22 (Fibriansah et al., 2015). Competition, intermediate competition, or no competition of binding was defined as described in Fig. 1 A.

#### Focus reduction neutralization test (FRNT)

Vero cells ( $3 \times 10^5$  cells/ml) were seeded in 96-well plates at 100 liters per well. The next day, mAbs were serially diluted in infection media and incubated with  $10^2$  FFU of specific SINV-VEEV subtypes for 1 h at 37°C. Antibody-virus complexes were added to Vero cell monolayers and incubated for 1 h at 37°C in duplicate wells. Subsequently, cells were overlaid with 1% methylcellulose in MEM (Invitrogen) supplemented with 100 U/ml penicillin, 100 U/ml streptomycin, 10 mM Hepes, 2 mM L-glutamine (Invitrogen), and 2% heat-inactivated FBS (Omega Scientific). Plates were fixed 18 h after virus inoculation with 1% paraformaldehyde (PFA) in D-PBS for 1 h at room temperature. After three washes with D-PBS-T, plates were incubated with 1  $\mu$ g/ml of anti-VEEV mAb 3B4C-4 (Roehrig and Mathews, 1985) diluted in permeabilization buffer (D-PBS, 0.1% saponin, and 0.1% BSA) for 1 h at room temperature or overnight at 4°C. Primary mAb was removed after three D-PBS-T washes, and plates were incubated with secondary HRP-conjugated goat anti-mouse IgG mAb (Sigma-Aldrich) in permeabilization buffer for 1 h at room temperature. Virus-infected foci were developed using TrueBlue peroxidase substrate (KPL) and counted using an ImmunoSpot 5.0.37 Macroanalyzer (Cellular Technology). Foci from wells containing virus incubated with mAb were compared to wells inoculated in the absence of mAb. Antibody dose-response curves were analyzed using nonlinear regression analysis with a variable slope constraining the bottom to 0 and top to 100 (GraphPad Software).

#### Binding to VEEV structural proteins via cell surface display

Transient transfection of Expi293F cells with plasmids containing the structural proteins (capsid-p62-6K-E1) of VEEV subtype IAB (strains TrD, TC-83), VEEV subtype IC (strain P676), VEEV subtype ID (strain 3880), VEEV subtype IE (strains Mena II; MX01-22), Mosso das Pedras virus (VEEV subtype IF [strain 78V-3531]), Everglades virus (VEEV subtype II [strain Fe3-7C]), Mucambo virus (VEEV subtype IIIA [strain BeAn 8]), VEEV subtype IIIC (strain 71D-1252), Pixuna virus (VEEV subtype IV [strain BeAr 35645]), Cabassou virus (VEEV subtype V [strain CaAr 508]), Rio Negro virus (VEEV subtype VI [strain Ag80-663]), WEEV (strain McMilian), or CHIKV (strain 181/25) was performed using the ExpiFectamine 293 transfection kit

(Gibco) according to the manufacturer's protocol as previously described (Williamson et al., 2021). Cells were incubated at 37°C in a humidified atmosphere of 8% CO<sub>2</sub> and harvested 24 h after transfection via centrifugation at 400 g for 5 min. Cells were resuspended in Expi293F expression medium (Gibco) and 10% DMSO for storage at -80°C or in the vapor phase of liquid nitrogen. Untransfected Expi293F cells served as a negative control for nonspecific mAb binding and were used fresh after incubation at 37°C in a humidified atmosphere of 8% CO<sub>2</sub> at 125 rpm. For analysis of mAb binding, cryopreserved cells were thawed and washed twice with D-PBS, 2% FBS, and 2 mM EDTA (FACS buffer). Cells were plated at 25,000–50,000 cells/well in 96-well V-bottom plates (Corning). Murine or human mAbs were diluted to 10  $\mu$ g/ml or 1:500 in FACS buffer and incubated with the cells for 30 min at 4°C. Cells were washed with FACS buffer and then incubated with secondary Abs (anti-mouse IgG-PE [Southern Biotech] or anti-human IgG-PE [Southern Biotech]) diluted 1:1,000 in FACS buffer for 30 min at 4°C. Cells were washed with FACS buffer and resuspended in 1:1,000 dilution of DAPI stain in FACS buffer at 25–30  $\mu$ l/well. The numbers of events were collected on an IntelliCy iQue Screener PLUS flow cytometer (Sartorius). For analysis, binding of the mAb to untransfected Expi293F was subtracted to account for any nonspecific mAb binding. Fold-change for mAb binding to the different alphavirus subtypes was calculated by normalization of the median fluorescence relative to the negative control human mAb, rDENV-2D22.

#### mAb binding to alphavirus-infected cells

Vero cells were seeded 1 d in advance into T-25 flasks (or 6-well plates pending scale of screening repeat) at  $3 \times 10^5$  cells/ml. Alphaviruses were diluted to an MOI of 1 in a small volume (enough to coat plate bottom) of infection media and added to cell monolayers for 1 h at 37°C to allow for virus attachment. Additional medium was added per flask size specifications, and infection proceeded for 20–22 h. Cells were rinsed with D-PBS, detached with TrypLE (Thermo Fisher Scientific), and resuspended in FACS buffer. Cells ( $4 \times 10^4$  per well) were transferred to a 96-well U-bottom plate and incubated for 1 h at 4°C with 10  $\mu$ g/ml of mAb diluted in FACS buffer. After two washes with FACS buffer, cells were incubated with an Alexa Fluor 647-conjugated goat anti-mouse or anti-human IgG (Invitrogen) diluted 1:2,000 in FACS buffer for 1 h at 4°C. Cells were fixed with 1% PFA in D-PBS for 10 min and resuspended in FACS buffer for processing. Antibody binding was measured by flow cytometry using a MACSQuant analyzer (Miltenyi Biotec) and analyzed using FlowJo software (TreeStar). Infectivity was scored as a percentage of Alexa Fluor 647-positive cells compared with mock-infected cells stained with the same mAb.

#### Attachment inhibition assay

Vero or  $\Delta B4galt7$  N2a cells were seeded into a 24-well plate at  $1.5 \times 10^5$  cells per well 1 d before the binding assay. SINV-VEEV TrD at an MOI of 1 was incubated for 1 h at 37°C with 10  $\mu$ g/ml (Vero cells) or 20  $\mu$ g/ml ( $\Delta B4galt7$  N2a cells) anti-VEEV mAbs in 200  $\mu$ l infection media. LDLRAD3-D1-Fc was used as a positive control for attachment inhibition on  $\Delta B4galt7$  N2a cells. BSA diluted



in D-PBS was used as a negative control for attachment inhibition on Vero cells, and murine and human isotype mAbs were used for comparison on both Vero and  $\Delta B4galt7$  N2a cells. For Vero cells, the mAb:virus mixture was cooled for 15 min at 4°C. Concurrently, cells were incubated with cold medium for 15 min at 4°C. Medium was removed from cells, and chilled mAb:virus mixtures were added to cells for 1 h at 4°C. Nonadsorbed virus was removed with six washes of 0.5 ml chilled infection media and vacuum aspiration. For  $\Delta B4galt7$  N2a cells, the mAb:virus mixture was added to cells for 2 h at room temperature. Nonadsorbed virus was removed with 10 washes of 1 ml of infection media at room temperature using vacuum aspiration. Sample RNA was processed using the KingFisher Flex system (Thermo Fisher Scientific) and analyzed by RT-qPCR using a TaqMan RNA-to-CT 1-Step Kit (Thermo Fisher Scientific). SINV-VEEV TrD RNA was quantitated and normalized to human *GAPDH* (Vero cells) or mouse *Gapdh* ( $\Delta B4galt7$  N2a cells). Primers and probes used are as follows: SINV nsP4 FWD, 5'-AAGATCATC GACGCAGTCATC-3'; SINV nsP4 REV, 5'-GCTGTGGAAGTAACC GAATCT-3'; SINV nsP4 Probe, 5'-/56-FAM/CCACCTTAC/ZEN/TTCTGCGGCGGATTTA/3IAbkFQ/-3'; human *GAPDH* (IDT; Hs.PT. 39a.22214838); mouse *Gapdh* (IDT; Mm. PT. 39a.1).

#### LDLRAD3-D1-Fc competition binding ELISA

For human LDLRAD3-D1-Fc (human IgG1) competition binding with murine anti-VEEV mAbs, Nunc MaxiSorp plates (Thermo Fisher Scientific) were coated with 2 µg/ml mouse capture mAb (mouse VEEV-1A4A; Roehrig and Mathews, 1985) in 100 µl of coating buffer (0.1 M Na<sub>2</sub>CO<sub>3</sub> and 0.02% NaN<sub>3</sub>, pH 9.6) and incubated overnight at 4°C. Plates were washed four times with D-PBS and incubated with 150 µl of blocking buffer for 1 h at room temperature. VEEV TC-83 VLPs were diluted to 1 µg/ml in D-PBS containing 2% BSA and added (100 µl/well) to plates for 1 h at room temperature. After four additional D-PBS washes, 50 µl of mouse anti-VEEV mAb at 20 µg/ml in D-PBS with 2% BSA was added to plates for 30 min at room temperature to allow for binding to VEEV TC-83 VLPs. 50 µl of human LDLRAD3-D1-Fc at 20 µg/ml then was added directly, with no additional washes. Plates were washed four times with D-PBS and incubated with 100 µl/well, 1:5,000 HRP-conjugated goat anti-human IgG (H + L; Jackson ImmunoResearch) diluted in D-PBS with 2% BSA for 1 h at room temperature for detection of human LDLRAD3-D1-Fc binding. Plates were processed as described above. For murine LDLRAD3-D1-Fc (murine IgG2b) competition with human anti-VEEV mAb hVEEV-63, the protocol was the same as above except a mixture of cross-reactive human CHIKV DC2.112 and DC2.315 mAbs (Kim et al., 2021; Quiroz et al., 2019) was used as capture mAbs, and HRP-conjugated goat anti-mouse IgG (H + L; Jackson ImmunoResearch) was used for detection of murine LDLRAD3-D1-Fc.

#### Virus FFWO inhibition assay

Vero cells ( $3 \times 10^4$  cells per well) were seeded in 96-well plates at 100 µl per well 1 d before infection. On the day of infection, 100 µl per well of 4°C binding medium (RPMI 1640, 10 mM Hepes, 0.2% BSA, and 20 mM NH<sub>4</sub>Cl) was added to Vero cell monolayers. Plates were kept on ice for 15 min. VEEV TC-83, diluted in cold binding medium, was added to the Vero cell

monolayer at a MOI of 20 for 1 h at 4°C. Unbound virus was removed after two washes with 4°C binding medium. 100 µl mAbs diluted to 10 µg/ml in infection media 1 h at 4°C. Unbound mAb was removed after two washes with 4°C binding medium. FFWO was induced by pulsing cells with low-pH fusion medium (RPMI 1640 + 10 mM Hepes, 0.2% BSA, and 30 mM succinic acid, adjusted to pH 5.5) for 2 min at 37°C. A no-fusion control was including using neutral-pH fusion medium (RPMI 1640 + 10 mM Hepes and 0.2% BSA, adjusted to pH 7.4). After the pulse, cells were washed twice and incubated with growth medium supplemented with 20 mM NH<sub>4</sub>Cl to prevent further infection via endocytosis. Infection proceeded for 5 h. Cells were rinsed with D-PBS, detached using TrypLE (Thermo Fisher Scientific), resuspended in FACS buffer, and fixed with 1% PFA in D-PBS for 8 min. After two washes with permeabilization buffer, cells were stained with 10 µg/ml of anti-VEEV mAb 3B4C-4 diluted in permeabilization buffer for 1 h at 4°C. Cells were washed twice more with permeabilization buffer and stained with a 1:2,000 dilution of Alexa Fluor 647-conjugated goat anti-mouse (Invitrogen) for 1 h at 4°C. After two washes with permeabilization buffer, cells were resuspended in FACS buffer. Infection was quantitated by flow cytometry using a MACSQuant analyzer (Miltenyi Biotec) and analyzed using FlowJo software (TreeStar). Infectivity was scored as a percentage of Alexa Fluor 647-positive cells compared with no-fusion control samples.

#### Virus egress inhibition assay

Vero cells ( $3 \times 10^5$  cells) were seeded in individual wells of a 12-well plate 1 d before infection. The next day, cells were inoculated with SINV-VEEV TrD at an MOI of 1 diluted in prewarmed infection media for 2 h at 37°C. Cells were then washed six times with prewarmed infection media to remove free virus in the supernatant. Anti-VEEV mAbs were diluted to 10 µg/ml in prewarmed basic medium (RPMI 1640, 2% FBS [Omega Scientific], 100 U/ml penicillin, 100 U/ml streptomycin, and 25 mM NH<sub>4</sub>Cl) to prevent reinfection. Cell supernatant (200 µl) was collected 1 h after mAb addition, frozen at -80°C, and replaced with 200 µl of additional mAb, diluted in prewarmed basic medium. Supernatant was also collected 6 h after mAb addition and frozen at -80°C. Viral RNA from supernatant was extracted using a MagMAX Viral RNA KingFisher Flex system (Thermo Fisher Scientific), analyzed by RT-qPCR, and compared to a predetermined SINV-VEEV TrD standard curve to determine FFU equivalents. The values were normalized to the volume of supernatant used for extraction.

#### Alanine-scanning mutagenesis epitope mapping

A pcDNA3.1(+) plasmid expressing codon-optimized VEEV TrD p62-6K-E1 structural genes was synthesized and mutagenized by Genewiz. Each residue of the VEEV E2 protein ectodomain (S1-Y363) was mutated to alanine, and alanine codons were mutated to serine. Mutant plasmids were transfected into HEK-293T cells using Lipofectamine 3000 (Thermo Fisher Scientific). 1 d later, cells were fixed with 1% PFA, washed twice with permeabilization buffer, and incubated with mAbs at preoptimized concentrations for 1 h at 4°C. Cells were washed twice with permeabilization buffer, and anti-VEEV mAb binding was

detected using Alexa Fluor 647-conjugated goat anti-mouse or anti-human IgG (Thermo Fisher Scientific) diluted 1:2,000 in permeabilization buffer. After two washes, cells were re-suspended in FACS buffer and processed by flow cytometry on a MACSQuant Analyzer (Miltenyi Biotec) using FlowJo software. The percentage of positively stained cells was calculated relative to mock-transfected cells. Antibody reactivity against each mutant was compared to the wild-type p62-6K-E1. An oligoclonal mixture of all the anti-VEEV mouse mAbs was used to control for mutant E2 protein expression. Using previously described criteria (Smith et al., 2015), critical residues were defined as those with  $\leq 25\%$  (or  $\leq 15\%$  for mVEEV-43 and mVEEV-68) binding to an individual mAb but  $\geq 70\%$  binding to an oligoclonal pool of anti-VEEV mAbs.

### Escape mutant generation and sequence analysis of the E2 protein gene

Vero cells ( $9 \times 10^5$  cells) were seeded in each well of a 6-well plate. 1 d later, SINV-VEEV TrD (MOI of 0.1) was incubated with anti-VEEV mAbs or an isotype control mAb (final 1 or 10  $\mu\text{g}/\text{ml}$ ) in infection media for 1 h at  $37^\circ\text{C}$ . Each mAb was first tested at 1  $\mu\text{g}/\text{ml}$ . Virus-mAb complexes were added to Vero cells in duplicate and incubated at  $37^\circ\text{C}$ . The next day, half of the cell supernatant was frozen at  $-80^\circ\text{C}$ , and half was incubated with freshly diluted anti-VEEV mAb (final 1 or 10  $\mu\text{g}/\text{ml}$ ) for 1 h at  $37^\circ\text{C}$  before being added to fresh Vero cells. This process was repeated for 6 d. If cytopathogenic effects were recorded 1 d after mAb addition, the virus was not adequately neutralized, and the assay was repeated with a higher dose of selection mAb at 10  $\mu\text{g}/\text{ml}$ . Cytopathogenic effects caused by an escape virus pool typically were first observed 2–3 d after infection. Escape mutants were confirmed using FRNT. Viral RNA was isolated from bulk virus supernatant pools using a QIAamp Viral RNA Mini kit (Qiagen) and processed using deep sequencing. Viral RNA from cell culture supernatants was used to generate shotgun sequencing libraries using either the Illumina TruSeq Stranded Total RNA Library Prep with Ribo-Zero kit or the Illumina Stranded Total RNA Prep with ligation with Ribo-Zero Plus kit per the manufacturer's protocol. The final indexed libraries were quantified using Agilent's Bioanalyzer and pooled at an equal molar concentration. Illumina's NextSeq sequencer was used to generate paired-end 150-bp reads. Raw sequencing data were processed using fastp (Chen et al., 2018) v0.20.1 (<https://github.com/OpenGene/fastp>) to trim adaptors and filter out sequences with  $< Q30$ . Alignment to genes encoding the structural proteins of VEEV TrD (EEVNSPEPA) was performed using BWA (Heng and Durbin, 2009) v0.7.17-r1188 (<http://bio-bwa.sourceforge.net>). LoFreq v2 (<https://csb5.github.io/lofreq/>) was used to call variants with an allele frequency  $\geq 50\%$ . Variants were annotated using SNPEff (Cingolani et al., 2012) 5.0c (<https://sourceforge.net/projects/snpeff/>). Sequence-identified escape mutations were introduced into the codon-optimized p62-6K-E1 genes of VEEV TrD, transfected, and screened for loss of VEEV mAb binding by flow cytometry as defined above.

### Negative stain grid preparation and imaging

For screening and imaging of negatively stained VEEV TC-83 VLP or VEEV-TC-83 VLP:VEE-63 Fab samples,  $\sim 3 \mu\text{l}$  of the

sample at concentrations of 10–15  $\mu\text{g}/\text{ml}$  was applied to glow-discharged grid with continuous carbon film on 400-square-mesh copper EM grids (Electron Microscopy Sciences). The grids were stained with 0.75% uranyl formate (Ohi et al., 2004). Images were recorded on a  $4\text{K} \times 4\text{K}$  CCD camera using an FEI TF20 (TFS) transmission electron microscope operated at 200 keV and controlled with SerialEM (Mastronarde, 2005). All images were taken at  $50,000\times$  magnification with a pixel size of 2.18  $\text{\AA}/\text{pixel}$  in low-dose mode at a defocus of 1.5–1.8  $\mu\text{m}$ . Image processing was performed using the cryoSPARC (Punjani et al., 2017).

### Cryo-EM sample preparation and data collection

hVEEV-63 Fab molecules were produced by digesting recombinant chromatography-purified IgG using resin-immobilized cysteine protease enzyme (FabALACTICA; Genovis). The digestion occurred in 100 mM sodium phosphate and 150 mM NaCl, pH 7.2 in D-PBS for  $\sim 16$  h at ambient temperature. To remove cleaved Fc from intact IgG, the digestion mix was incubated with CaptureSelect Fc resin (Genovis) for 30 min at ambient temperature in D-PBS. For the VEEV TC-83 VLP:hVEEV-63 Fab complex, purified VEEV TC-83 VLP was concentrated to 5 mg/ml and mixed with hVEEV-63 Fab (4.4 mg/ml) at a molar ratio of 720:1 (Fab:VLP). The mixture was incubated for 1 h at ambient temperature, and buffer exchanged with Amicon 100 kD centrifugal filter units (Millipore Sigma; 25 mM Hepes, pH 7.5, 100 mM NaCl, and 2 mM EDTA). VEEV TC-83 VLP or VEEV TC-83 VLP:hVEEV-63 Fab (2.2  $\mu\text{l}$ ) samples were applied twice to glow discharged (40 s at 25 mA) 300-mesh Lacey grids. The grid was blotted for 2 s before plunging into liquid ethane using a FEI Vitrobot Mark4 (TFS) at  $8^\circ\text{C}$  and 100% humidity. Grids were imaged on a Titan Krios (TFS) microscope operated at 300 keV equipped with a Falcon 4 (TFS) DED camera using counting mode. Datasets were collected for each sample (VEEV TC-83 VLP or VEEV TC-83 VLP:hVEEV-63 Fab). Movies were collected at a nominal magnification of  $75,000\times$ , pixel size of 1.02775  $\text{\AA}/\text{px}$ , and defocus range of 0.5–1.6  $\mu\text{m}$ . Grids were exposed at  $1\text{e}^-/\text{\AA}^2/\text{frame}$  over 40 frames, resulting in a total dose of  $\sim 40\text{e}^-/\text{\AA}^2$  (Fig. S4 and Table S3).

### Cryo-EM data processing

Videos were preprocessed with MotionCorr2 (Zheng et al., 2017) and Gctf (Zhang, 2016), using RELION (Fernandez-Leiro and Scheres, 2017). Micrographs with low resolution, high astigmatism, and defocus were removed from the data set. Further processing was done using RELION 3.1 and was the same for both datasets unless specified. A small subset of micrographs was autopicked first by RELION LoG (Fernandez-Leiro and Scheres, 2017), and 2D class averages were determined. Representative classes were selected and used as templates for another round of autopicking. The particles were extracted in a box size of 1,200 pixels and binned by 2 to a pixel size of 2.05  $\text{\AA}/\text{pixel}$ . The particles were then subjected to multiple rounds of 2D class averages and 3D classification (with and without symmetry) to obtain a set of clean and homogeneous particles. The particles from the selected classes were re-extracted at a pixel size of 1.806  $\text{\AA}/\text{pixel}$ , 3D classified, and subjected to 3D autorefinement.

The data were further processed with CTFrefine and polished, and final postprocessing was performed. The final dataset was expanded by *I* symmetry and 3D classified with a mask over the asymmetric unit. The particles from the selected classes were re-extracted with the full pixel size (1.027 Å). The asymmetric unit was subjected to particle subtraction and 3D autorefinement with masking. Detailed statistics are provided in Fig. S4 and Table S3.

### Model building

For the VEEV TC-83 VLP complex, a homology model of the VEEV vaccine strain, TC-83 (PDB ID 3JOC; Zhang et al., 2011), was used for docking to the cryo-EM map with Chimera rigid body fit and Phenix (Adams et al., 2010; Pettersen et al., 2004). To improve the coordinate fitting, the model was subjected to iterative refinement of manual building in Coot (Emsley and Cowtan, 2004) and Phenix real-space refinement (Adams et al., 2010). The model was validated with Molprobtity (Chen et al., 2010). For the VEEV TC-83 VLP:hVEEV-63 Fab complex, a homology model for the Fab (PDB ID 12E8) and the refined model of the VEEV TC-83 VLP were used as starting model. The models were docked to the cryo-EM map with Chimera rigid body fit. The model was then refined in Phenix (phenix real-space refinement) and Coot. The model was validated by Molprobtity (Table S3).

### Mouse studies

Immunocompetent 6-wk-old female CD-1 mice (Charles River) were administered 100 µg of anti-VEEV mAb or isotype control mAb via an i.p. route 24 h before or after challenge. Mice were inoculated with a target 50 PFU of VEEV TrD V3000 or a nanoluciferase-expressing version, VEEV TrD nanoLuc TaV (Sun et al., 2014), via an aerosol route. Aerosol exposures were performed as previously described using the AeroMP exposure system (Biaera Technologies) inside a biological safety cabinet class III (Reed et al., 2016). Briefly, mice were placed inside a whole-body aerosol exposure chamber inside the class III cabinet and exposed for 10 min to an aerosol-containing VEEV generated by a Collison 3-jet nebulizer (CH Technologies). The nebulizer was operated at 7.5 lpm, 25–30 psi. Total air into and out of the chamber during the exposure was 19.5 lpm to achieve 1 full air change in the chamber every 2 min. Aerosol samples were collected in an all-glass impinger (AGI 7541; Ace Glass) operated at 6 lpm, –5 to –11 psi, to determine inhaled dose. After a 5-min air wash, mice were returned to their cages. Infected mice were observed daily for 14 d after inoculation, weighed, and assessed for mortality. 5 d after challenge, some mice were injected i.p. with 10 µg Nano-Glo substrate (Promega) in DPBS. After a 4-min incubation, the dorsal cranium was imaged using an IVIS SpectrumCT In Vivo Imaging System (PerkinElmer) at 405 nm. The total flux (photons · s<sup>–1</sup>) in the head region, taken as a measure of brain replication, was calculated for animals in each treatment group based on the radiance (photons · s<sup>–1</sup> · cm<sup>2</sup> · sr<sup>–1</sup>) and was quantified using Living Image software (PerkinElmer). The dynamic range of the IVIS imager signal from the heads of uninfected mice to highly infected mice was ~100-fold (~1–2 × 10<sup>5</sup> to ~1–2 × 10<sup>7</sup> photons · s<sup>–1</sup>, respectively). Sample sizes were

estimated to determine a 50% reduction in lethality after mAb treatment. Blinding and randomization were not performed.

### Statistical analysis

Statistical significance was assigned when *P* values were <0.05 using Prism v9 (GraphPad). One-way ANOVA multiple comparisons test, unpaired *t* test, Mann-Whitney *U* tests, and log-rank tests, number of animals (*n*), median values, and statistical comparison groups are indicated in the figure legends.

### Materials availability

All requests for resources and reagents, including mice, antibodies, and proteins, should be directed to the co-corresponding authors. All reagents will be made available on request after completion of a Materials Transfer Agreement.

### Online supplemental material

Fig. S1 shows anti-VEEV mAbs target E2 and the cross-reactivity of anti-VEEV mAbs to different alphaviruses. Fig. S2 shows E2 glycoprotein amino acid sequence identity of alphaviruses used in this study. Fig. S3 provides an amino acid sequence alignment of the E2 glycoproteins of alphaviruses used in this study. Fig. S4 depicts a flow chart of cryo-EM processing steps of the maps of VEEV TC-83 VLP and VEEV TC-83 VLP:hVEEV-63 Fab complex. Table S1 shows comprehensive alanine scanning mutagenesis results for anti-VEEV mAbs and corresponding mutations in the VEEV TrD E2 glycoprotein. Table S2 lists VEEV TC-83 E2 variants identified in antibody escape mutation pools. Table S3 shows statistical parameters used for high-resolution data collection of VEEV TC-83 VLP and VEEV TC-83 VLP:hVEEV-63 Fab.

### Data availability

All data and sequences supporting the findings of this study are available within the paper and from the corresponding author upon request. Structural datasets have been uploaded and are available at PDB and EMDB (PDB IDs 7SFU, 7SFV, and 7SFW; EMDB IDs EMD-25102, EMD-25103, and EMD-25104).

### Acknowledgments

We thank Katherine O'Malley, Zachary Ryckman, and Morgan Midgett for assistance in performing VEEV aerosol challenge experiments in mice. The graphical abstract was created using BioRender.com.

This study was supported by National Institutes of Health grants R01 AI095436 (W.B. Klimstra), U19 AI142790 (J.E. Crowe and M.S. Diamond), T32 AI007172 (N.M. Kafai), T32 HL069765 (L.E. Williamson), F31 AI145189 (L.E. Williamson), and U01 AI151810 (M.S. Diamond, S.A. Handley); the Defense Threat Reduction Agency grants HDTRA1-15-1-0013 (M.S. Diamond, W.B. Klimstra, and D.S. Reed) and HDTRA1-13-1-0034 (J.E. Crowe); and the 2019 Future Insight Prize from Merck (J.E. Crowe). Data collection was performed at the Stanford-SLAC National Accelerator Laboratory Cryo-EM Center (S<sup>2</sup>C<sup>2</sup>) supported by the National Institutes of Health Common Fund Transformative High Resolution Cryo-Electron Microscopy program (U24 GM129541).



Author contributions: S. Sukupolvi-Petty generated murine mAb hybridomas. N.M. Kafai generated recombinant proteins and performed mAb neutralization, mechanism, and mapping experiments. L.E. Williamson generated human mAb hybridomas and recombinant proteins, performed competition binding studies, and VEE antigenic complex surface binding cross-reactivity experiments. N.M. Kafai and J. Liu performed alpha-virus cross-reactivity experiments. A.S. Kim designed and generated recombinant VEEV TC-83 E2. E. Binshtein performed cryo-EM reconstructions and asymmetric unit atomic modeling. A. Jung, S.A. Handley, and L. Droit performed shotgun sequencing analysis on viral stocks and viral escape pools. C.L. Gardner and D.S. Reed performed in vivo experiments. N.M. Kafai, L.E. Williamson, S. Sukupolvi-Petty, C.L. Gardner, E. Binshtein, J. Liu, A.S. Kim, N. Kose, R.H. Carnahan, S.A. Handley, W.B. Klimstra, J.E. Crowe, and M.S. Diamond designed experiments. N.M. Kafai, L.E. Williamson, S. Sukupolvi-Petty, C.L. Gardner, E. Binshtein, J. Liu, and S.A. Handley performed sequence data analysis. N.M. Kafai, L.E. Williamson, and M.S. Diamond wrote the initial draft, with the other authors providing comments.

Disclosures: M.S. Diamond is a consultant for Inbios, Vir Biotechnology, and Carnival Corporation, and on the Scientific Advisory Boards of Moderna and Immunome. The Diamond laboratory has received funding support in sponsored research agreements from Moderna, Vir Biotechnology, and Emergent BioSolutions. Washington University has licensed murine anti-VEEV mAbs, and M.S. Diamond, S. Sukupolvi-Petty, and N.M. Kafai are inventors. J.E. Crowe has served as a consultant for Luna Biologics, is a member of the Scientific Advisory Boards of Meissa Vaccines, and is founder of IDBiologics. The Crowe laboratory has received unrelated sponsored research agreements from Takeda, AstraZeneca, and IDBiologics. J.E. Crowe reported grants from NIH during the conduct of the study and from GSK and Merck and grants from IDBiologics outside the submitted work; in addition, J. Crowe had a patent app for human antibodies for VEEV pending. The Klimstra laboratory has received unrelated research support from SAB Biotherapeutics and Tiba Biotechnology. The other authors have no additional conflicts of interest to declare. No other disclosures were reported.

Submitted: 21 December 2021

Revised: 31 January 2022

Accepted: 1 February 2022

## References

- Adams, P.D., P.V. Afonine, G. Bunkoczi, V.B. Chen, I.W. Davis, N. Echols, J.J. Headd, L.W. Hung, G.J. Kapral, R.W. Grosse-Kunstleve, et al. 2010. PHENIX: A comprehensive python-based system for macromolecular structure solution. *Acta Crystallogr. Sect. D Biol. Crystallogr.* 66:213–221. <https://doi.org/10.1107/S09074449090052925>
- Agapov, E.V., I.A. Razumov, I.V. Frolov, A.A. Kolykhalov, S.V. Netesov, and V.B. Loktev. 1994. Localization of four antigenic sites involved in Venezuelan equine encephalomyelitis virus protection. *Arch. Virol.* 139: 173–181. <https://doi.org/10.1007/BF01309462>
- Aguilar, P.V., J.G. Estrada-Franco, R. Navarro-Lopez, C. Ferro, A.D. Haddow, and S.C. Weaver. 2011. Endemic Venezuelan equine encephalitis in the Americas: Hidden under the dengue umbrella. *Future Virol.* 6:721–740. <https://doi.org/10.2217/FVL.11.5>
- Aguilar, P.V., I.P. Greene, L.L. Coffey, G. Medina, A.C. Moncayo, M. Anishchenko, G.V. Ludwig, M.J. Turell, M.L. O'Guinn, J. Lee, et al. 2004. Endemic Venezuelan equine encephalitis in northern Peru. *Emerg. Infect. Dis.* 10:880–888. <https://doi.org/10.3201/eid1005.030634>
- Anishchenko, M., R.A. Bowen, S. Paessler, L. Austgen, I.P. Greene, and S.C. Weaver. 2006. Venezuelan encephalitis emergence mediated by a phylogenetically predicted viral mutation. *Proc. Natl. Acad. Sci. USA.* 103: 4994–4999. <https://doi.org/10.1073/pnas.0509961103>
- Anishchenko, M., S. Paessler, I.P. Greene, P.V. Aguilar, A.-S. Carrara, and S.C. Weaver. 2004. Generation and characterization of closely related epizootic and enzootic infectious cDNA clones for studying interferon sensitivity and emergence mechanisms of Venezuelan equine encephalitis virus. *J. Virol.* 78:1–8. <https://doi.org/10.1128/jvi.78.1.1-8.2004>
- Basore, K., H. Ma, N.M. Kafai, S. Mackin, A.S. Kim, C.A. Nelson, M.S. Diamond, and D.H. Fremont. 2021. Structure of Venezuelan equine encephalitis virus in complex with its LDLRAD3 receptor. *Nature.* 598: 672–676. <https://doi.org/10.1038/s41586-021-03963-9>
- Berge, T.O., I.S. Banks, and W.D. Tigertt. 1961. Attenuation of Venezuelan equine encephalomyelitis virus by in vitro cultivation in guinea pig heart cells. *Am. J. Epidemiol.* 73:209–218. <https://doi.org/10.1093/oxfordjournals.aje.a120178>
- Bernard, K.A., W.B. Klimstra, and R.E. Johnston. 2000. Mutations in the E2 glycoprotein of Venezuelan equine encephalitis virus confer heparan sulfate interaction, low morbidity, and rapid clearance from blood of mice. *Virology.* 276:93–103. <https://doi.org/10.1006/viro.2000.0546>
- Blosser, E.M., and N.D. Burkett-Cadena. 2017. Culex (Melanoconion) panocosa from peninsular Florida, USA. *Acta Trop.* 167:59–63. <https://doi.org/10.1016/j.actatropica.2016.12.024>
- Bond, C.S., and A.W. Schüttelkopf. 2009. ALINE: A WYSIWYG protein-sequence alignment editor for publication-quality alignments. *Acta Crystallogr. Sect. D Biol. Crystallogr.* 65:510–512. <https://doi.org/10.1107/S0907444909007835>
- Braut, A.C., A.M. Powers, D. Ortiz, J.G. Estrada-Franco, R. Navarro-Lopez, and S.C. Weaver. 2004. Venezuelan equine encephalitis emergence: Enhanced vector infection from a single amino acid substitution in the envelope glycoprotein. *Proc. Natl. Acad. Sci. USA.* 101:11344–11349. <https://doi.org/10.1073/pnas.0402905101>
- Bronze, M.S., M.M. Huycke, L.J. Machado, G.W. Voskuhl, and R.A. Greenfield. 2002. Viral agents as biological weapons and agents of bioterrorism. *Am. J. Med. Sci.* 323:316–325. <https://doi.org/10.1097/00000441-200206000-00004>
- Burke, C.W., J.W. Froude, F. Rossi, C.E. White, C.L. Moyer, J. Ennis, M.L. Pitt, S. Streatchfield, R.M. Jones, K. Musiyuchuk, et al. 2019. Therapeutic monoclonal antibody treatment protects nonhuman primates from severe Venezuelan equine encephalitis virus disease after aerosol exposure. *PLoS Pathog.* 15:e1008157. <https://doi.org/10.1371/journal.ppat.1008157>
- Byrnes, A.P., and D.E. Griffin. 2000. Large-plaque mutants of Sindbis virus show reduced binding to heparan sulfate, heightened viremia, and slower clearance from the circulation. *J. Virol.* 74:644–651. <https://doi.org/10.1128/jvi.74.2.644-651.2000>
- Calisher, C.H., F.A. Murphy, J.K. France, J.S. Lazuck, D.J. Muth, F. Steck, H.S. Lindsey, S.P. Bauer, E.E. Buff, and N.J. Schneider. 1980. Everglades virus infection in man, 1975. *South Med. J.* 73:1548. <https://doi.org/10.1097/00007611-198011000-00044>
- Casals, J., S.M. Buckley, and D.W. Barry. 1973. Resistance to arbovirus challenge in mice immediately after vaccination. *Appl. Microbiol.* 25:755–762. <https://doi.org/10.1128/am.25.5.755-762.1973>
- Chen, R.E., X. Zhang, J.B. Case, E.S. Winkler, Y. Liu, L.A. VanBlargan, J. Liu, J.M. Errico, X. Xie, N. Suryadevara, et al. 2021. Resistance of SARS-CoV-2 variants to neutralization by monoclonal and serum-derived polyclonal antibodies. *Nat. Med.* 27:717–726. <https://doi.org/10.1038/s41591-021-01294-w>
- Chen, S., Y. Zhou, Y. Chen, and J. Gu. 2018. fastp: an ultra-fast all-in-one FASTQ preprocessor. *Bioinformatics.* 34(17):i884–i890. <https://doi.org/10.1093/bioinformatics/bty560>
- Chen, V.B., W.B. Arendall 3rd, J.J. Headd, D.A. Keedy, R.M. Immormino, G.J. Kapral, L.W. Murray, J.S. Richardson, and D.C. Richardson. 2010. MolProbity: All-atom structure validation for macromolecular crystallography. *Acta Crystallogr. Sect. D Biol. Crystallogr.* 66:12–21. <https://doi.org/10.1107/S0907444909042073>
- Cingolani, P., A. Platts, L.W. Le, M. Coon, T. Nguyen, L. Wang, S.J. Land, X. Lu, and D.M. Ruden. 2012. A program for annotating and predicting the

- effects of single nucleotide polymorphisms, SnpEff. *Fly.* 6(2):80–92. <https://doi.org/10.4161/fly.19695>
- Davidson, E., and B.J. Doranz. 2014. A high-throughput shotgun mutagenesis approach to mapping B-cell antibody epitopes. *Immunology.* 143:13–20. <https://doi.org/10.1111/imm.12323>
- Earnest, J.T., K. Basore, V. Roy, A.L. Bailey, D. Wang, G. Alter, D.H. Fremont, and M.S. Diamond. 2019. Neutralizing antibodies against Mayaro virus require Fc effector functions for protective activity. *J. Exp. Med.* 216: 2282–2301. <https://doi.org/10.1084/jem.20190736>
- Edelman, R., M.S. Ascher, C.N. Oster, H.H. Ramsburg, F.E. Cole, and G.A. Eddy. 1979. Evaluation in humans of a new, inactivated vaccine for Venezuelan equine encephalitis virus (C-84). *J. Infect. Dis.* 140:708–715. <https://doi.org/10.1093/infdis/140.5.708>
- Emsley, P., and K. Cowtan. 2004. Coot: Model-building tools for molecular graphics. *Acta Crystallogr. Sect. D Biol. Crystallogr.* 60:2126–2132. <https://doi.org/10.1107/S0907444904019158>
- Fernandez-Leiro, R., and S.H.W. Scheres. 2017. A pipeline approach to single-particle processing in RELION. *Acta Crystallogr. D Struct. Biol.* 73: 496–502. <https://doi.org/10.1107/S2059798316019276>
- Fibriansah, G., K.D. Ibarra, T.S. Ng, S.A. Smith, J.L. Tan, X.N. Lim, J. S. G. Ooi, V.A. Kostyuchenko, J. Wang, A.M. de Silva, et al. 2015. DENGUE VIRUS. Cryo-EM structure of an antibody that neutralizes dengue virus type 2 by locking E protein dimers. *Science.* 349:88–91. <https://doi.org/10.1126/science.aaa8651>
- Forrester, N.L., J.O. Wertheim, V.G. Dugan, A.J. Auguste, D. Lin, A.P. Adams, R. Chen, R. Gorchakov, G. Leal, J.G. Estrada-Franco, et al. 2017. Evolution and spread of Venezuelan equine encephalitis complex alphavirus in the Americas. *PLoS Negl. Trop. Dis.* 11:e0005693. <https://doi.org/10.1371/journal.pntd.0005693>
- Fox, J.M., F. Long, M.A. Edeling, H. Lin, M.K.S. Van Duijl-Richter, R.H. Fong, K.M. Kahle, J.M. Smit, J. Jin, G. Simmons, et al. 2015. Broadly neutralizing alphavirus antibodies bind an epitope on E2 and inhibit entry and egress. *Cell.* 163:1095–1107. <https://doi.org/10.1016/j.cell.2015.10.050>
- Gardner, C.L., G.D. Ebel, K.D. Ryman, and W.B. Klimstra. 2011. Heparan sulfate binding by natural eastern equine encephalitis viruses promotes neurovirulence. *Proc. Natl. Acad. Sci. USA.* 108:16026–16031. <https://doi.org/10.1073/pnas.1110617108>
- Gardner, C.L., C. Sun, T. Luke, K. Raviprakash, H. Wu, J.A. Jiao, E. Sullivan, D.S. Reed, K.D. Ryman, and W.B. Klimstra. 2017. Antibody preparations from human transchromosomal cows exhibit prophylactic and therapeutic efficacy against Venezuelan equine encephalitis virus. *J. Virol.* 91: e00226–17. <https://doi.org/10.1128/JVI.00226-17>
- Gilbert, J.M., and H.B. Greenberg. 1997. Virus-like particle-induced fusion from without in tissue culture cells: Role of outer-layer proteins VP4 and VP7. *J. Virol.* 71:4555–4563. <https://doi.org/10.1128/JVI.71.6.4555-4563.1997>
- Goodchild, S.A., L.M. O'Brien, J. Steven, M.R. Muller, O.J. Lanning, C.H. Logue, R.V. D'Elia, R.J. Phillpotts, and S.D. Perkins. 2011. A humanised murine monoclonal antibody with broad serogroup specificity protects mice from challenge with Venezuelan equine encephalitis virus. *Antivir. Res.* 90:1–8. <https://doi.org/10.1016/j.antiviral.2011.01.010>
- Guzmán-Terán, C., A. Calderón-Rangel, A. Rodríguez-Morales, and S. Mattar. 2020. Venezuelan equine encephalitis virus: The problem is not over for tropical America. *Ann. Clin. Microbiol. Antimicrob.* 19:19. <https://doi.org/10.1186/s12941-020-00360-4>
- Hawley, R.J., and E.M. Eitzen Jr. 2001. Biological weapons—a primer for microbiologists. *Annu. Rev. Microbiol.* 55:235–253. <https://doi.org/10.1146/annurev.micro.55.1.235>
- Heng, L., and R. Durbin. 2009. Fast and accurate short read alignment with Burrows-Wheeler transform. *Bioinformatics.* 25(14):1754–1760. <https://doi.org/10.1093/bioinformatics/btp324>
- Hu, W.G., D. Chau, J. Wu, S. Jager, and L.P. Nagata. 2007. Humanization and mammalian expression of a murine monoclonal antibody against Venezuelan equine encephalitis virus. *Vaccine.* 25:3210–3214. <https://doi.org/10.1016/j.vaccine.2007.01.034>
- Hülseweh, B., T. Rülker, T. Pelat, C. Langermann, A. Frenzel, T. Schirrmann, S. Dübel, P. Thullier, and M. Hust. 2014. Human-like antibodies neutralizing Western equine encephalitis virus. *mAbs.* 6:717–726. <https://doi.org/10.4161/mabs.28170>
- Hunt, A.R., R.A. Bowen, S. Frederickson, T. Maruyama, J.T. Roehrig, and C.D. Blair. 2011. Treatment of mice with human monoclonal antibody 24h after lethal aerosol challenge with virulent Venezuelan equine encephalitis virus prevents disease but not infection. *Virology.* 414:146–152. <https://doi.org/10.1016/j.virol.2011.03.016>
- Hunt, A.R., S. Frederickson, C. Hinkel, K.S. Bowdish, and J.T. Roehrig. 2006. A humanized murine monoclonal antibody protects mice either before or after challenge with virulent Venezuelan equine encephalomyelitis virus. *J. Gen. Virol.* 87:2467–2476. <https://doi.org/10.1099/vir.0.81925-0>
- Hunt, A.R., S. Frederickson, T. Maruyama, J.T. Roehrig, and C.D. Blair. 2010. The first human epitope map of the alphaviral E1 and E2 proteins reveals a new E2 epitope with significant virus neutralizing activity. *PLoS Negl. Trop. Dis.* 4:e739. <https://doi.org/10.1371/journal.pntd.0000739>
- Hunt, A.R., and J.T. Roehrig. 1985. Biochemical and biological characteristics of epitopes on the E1 glycoprotein of western equine encephalitis virus. *Virology.* 142:334–346. [https://doi.org/10.1016/0042-6822\(85\)90342-3](https://doi.org/10.1016/0042-6822(85)90342-3)
- Jahrling, P.B., and E.H. Stephenson. 1984. Protective efficacies of live attenuated and formaldehyde-inactivated Venezuelan equine encephalitis virus vaccines against aerosol challenge in hamsters. *J. Clin. Microbiol.* 19:429–431. <https://doi.org/10.1128/jcm.19.3.429-431.1984>
- Jin, J., N.M. Liss, D.-H. Chen, M. Liao, J.M. Fox, R.M. Shimak, R.H. Fong, D. Chafets, S. Bakkour, and S. Keating. 2015. Neutralizing monoclonal antibodies block chikungunya virus entry and release by targeting an epitope critical to viral pathogenesis. *Cell Rep.* 13:2553–2564. <https://doi.org/10.1016/j.celrep.2015.11.043>
- Johnson, B. J., R.M. Kinney, C.L. Kost, and D.W. Trent. 1986. Molecular determinants of alphavirus neurovirulence: Nucleotide and deduced protein sequence changes during attenuation of Venezuelan equine encephalitis virus. *J. Gen. Virol.* 67(Pt 9):1951–1960. <https://doi.org/10.1099/0022-1317-67-9-1951>
- Kim, A.S., S.K. Austin, C.L. Gardner, A. Zuiani, D.S. Reed, D.W. Trobaugh, C. Sun, K. Basore, L.E. Williamson, J.E. Crowe, et al. 2019. Protective antibodies against Eastern equine encephalitis virus bind to epitopes in domains A and B of the E2 glycoprotein. *Nat. Microbiol.* 4:187–197. <https://doi.org/10.1038/s41564-018-0286-4>
- Kim, A.S., N.M. Kafai, E.S. Winkler, T.C. Gilliland, E.L. Cottle, J.T. Earnest, P.N. Jethva, P. Kaplonek, A.P. Shah, R.H. Fong, et al. 2021. Pan-protective anti-alphavirus human antibodies target a conserved E1 protein epitope. *Cell.* 184:4414–4429.e19. <https://doi.org/10.1016/j.cell.2021.07.006>
- Kinney, R.M., G.J. Chang, K.R. Tsuchiya, J.M. Sneider, J.T. Roehrig, T.M. Woodward, and D.W. Trent. 1993. Attenuation of Venezuelan equine encephalitis virus strain TC-83 is encoded by the 5'-noncoding region and the E2 envelope glycoprotein. *J. Virol.* 67:1269–1277. <https://doi.org/10.1128/JVI.67.3.1269-1277.1993>
- Kinney, R.M., J.J. Esposito, J.H. Mathews, B.J. Johnson, J.T. Roehrig, A.D. Barrett, and D.W. Trent. 1988. Recombinant vaccinia virus/Venezuelan equine encephalitis (VEE) virus protects mice from peripheral VEE virus challenge. *J. Virol.* 62:4697–4702. <https://doi.org/10.1128/JVI.62.12.4697-4702.1988>
- Kinney, R.M., B. J. Johnson, J.B. Welch, K.R. Tsuchiya, and D.W. Trent. 1989. The full-length nucleotide sequences of the virulent Trinidad donkey strain of Venezuelan equine encephalitis virus and its attenuated vaccine derivative, strain TC-83. *Virology.* 170:19–30. [https://doi.org/10.1016/0042-6822\(89\)90347-4](https://doi.org/10.1016/0042-6822(89)90347-4)
- Ko, S.Y., W. Akahata, E.S. Yang, W.P. Kong, C.W. Burke, S.P. Honnold, D.K. Nichols, Y. J. S. Huang, G.L. Schieber, K. Carlton, et al. 2019. A virus-like particle vaccine prevents equine encephalitis virus infection in non-human primates. *Sci. Transl. Med.* 11:eav3113. <https://doi.org/10.1126/scitranslmed.aav3113>
- León, B., C. Jiménez-Sánchez, and M. Retamosa-Izaguirre. 2020. An environmental niche model to estimate the potential presence of Venezuelan equine encephalitis virus in Costa Rica. *Int. J. Environ. Res. Public Health.* 18. <https://doi.org/10.3390/ijerph18010227>
- Lescar, J., A. Roussel, M.W. Wien, J. Navaza, S.D. Fuller, G. Wengler, G. Wengler, and F.A. Rey. 2001. The fusion glycoprotein shell of semliki forest virus: An icosahedral assembly primed for fusogenic activation at endosomal pH. *Cell.* 105:137–148. [https://doi.org/10.1016/S0092-8674\(01\)00303-8](https://doi.org/10.1016/S0092-8674(01)00303-8)
- Leung, J. Y. S., M. M. L. Ng, and J. J. H. Chu. 2011. Replication of alphaviruses: A review on the entry process of alphaviruses into cells. *Adv. Virol.* 2011: 249640. <https://doi.org/10.1155/2011/249640>
- Liao, M., and M. Kielian. 2005. Domain III from class II fusion proteins functions as a dominant-negative inhibitor of virus membrane fusion. *J. Cell Biol.* 171:111–120. <https://doi.org/10.1083/jcb.200507075>
- Ma, B., C. Huang, J. Ma, Y. Xiang, and X. Zhang. 2021. Structure of Venezuelan equine encephalitis virus with its receptor LDLRAD3. *Nature.* 598:677–681. <https://doi.org/10.1038/s41586-021-03909-1>
- Ma, H., A.S. Kim, N.M. Kafai, J.T. Earnest, A.P. Shah, J.B. Case, K. Basore, T.C. Gilliland, C. Sun, C.A. Nelson, et al. 2020. LDLRAD3 is a receptor for Venezuelan equine encephalitis virus. *Nature.* 588:308–314. <https://doi.org/10.1038/s41586-020-2915-3>



- Mastrorade, D.N. 2005. Automated electron microscope tomography using robust prediction of specimen movements. *J. Struct. Biol.* 152:36–51. <https://doi.org/10.1016/j.jsb.2005.07.007>
- Mathews, J.H., and J.T. Roehrig. 1982. Determination of the protective epitopes on the glycoproteins of Venezuelan equine encephalomyelitis virus by passive transfer of monoclonal antibodies. *J. Immunol.* 129: 2763–2767
- Morgan, I.M., R.W. Schlesinger, and P.K. Olitsky. 1942. Induced resistance of the central nervous system to experimental infection with equine encephalomyelitis virus: Neutralization antibody in the central nervous system in relation to cerebral resistance. *J. Exp. Med.* 76:357–369. <https://doi.org/10.1084/jem.76.4.357>
- Mukherjee, S., K.A. Dowd, C.J. Manhart, J.E. Ledgerwood, A.P. Durbin, S.S. Whitehead, and T.C. Pierson. 2014. Mechanism and significance of cell type-dependent neutralization of flaviviruses. *J. Virol.* 88:7210–7220. <https://doi.org/10.1128/JVI.03690-13>
- O'Brien, L.M., C.D. Underwood-Fowler, S.A. Goodchild, A.L. Phelps, and R.J. Philpotts. 2009. Development of a novel monoclonal antibody with reactivity to a wide range of Venezuelan equine encephalitis virus strains. *Virol. J.* 6:206. <https://doi.org/10.1186/1743-422X-6-206>
- Ohi, M., Y. Li, Y. Cheng, and T. Walz. 2004. Negative staining and image classification - powerful tools in modern electron microscopy. *Biol. Proced. Online.* 6:23–34. <https://doi.org/10.1251/bpo70>
- Oliphant, T., M. Engle, G.E. Nybakken, C. Doane, S. Johnson, L. Huang, S. Gorlatov, E. Mehlhop, A. Marri, K.M. Chung, et al. 2005. Development of a humanized monoclonal antibody with therapeutic potential against West Nile virus. *Nat. Med.* 11(5):522–530. <https://doi.org/10.1038/nm1240>
- Paessler, S., R.Z. Fayzulin, M. Anishchenko, I.P. Greene, S.C. Weaver, and I. Frolov. 2003. Recombinant Sindbis/Venezuelan equine encephalitis virus is highly attenuated and immunogenic. *J. Virol.* 77:9278–9286. <https://doi.org/10.1128/jvi.77.17.9278-9286.2003>
- Pal, P., K.A. Dowd, J.D. Brien, M.A. Edeling, S. Gorlatov, S. Johnson, I. Lee, W. Akahata, G.J. Nabel, M.K.S. Richter, et al. 2013. Development of a highly protective combination monoclonal antibody therapy against chikungunya virus. *PLoS Pathog.* 9(4). <https://doi.org/10.1371/journal.ppat.1003312>
- Pettersen, E.F., T.D. Goddard, C.C. Huang, G.S. Couch, D.M. Greenblatt, E.C. Meng, and T.E. Ferrin. 2004. UCSF Chimera: A visualization system for exploratory research and analysis. *J. Comput. Chem.* 25:1605–1612. <https://doi.org/10.1002/jcc.20084>
- Philpotts, R.J. 2006. Venezuelan equine encephalitis virus complex-specific monoclonal antibody provides broad protection, in murine models, against airborne challenge with viruses from serogroups I, II and III. *Virus Res.* 120:107–112. <https://doi.org/10.1016/j.virusres.2006.02.003>
- Philpotts, R.J., L.D. Jones, and S.C. Howard. 2002. Monoclonal antibody protects mice against infection and disease when given either before or up to 24 h after airborne challenge with virulent Venezuelan equine encephalitis virus. *Vaccine.* 20:1497–1504. [https://doi.org/10.1016/s0264-410x\(01\)00505-9](https://doi.org/10.1016/s0264-410x(01)00505-9)
- Porta, J., J. Jose, J.T. Roehrig, C.D. Blair, R.J. Kuhn, M.G. Rossmann, and T.S. Dermody. 2014. Locking and blocking the viral landscape of an alphavirus with neutralizing antibodies. *J. Virol.* 88:9616–9623. <https://doi.org/10.1128/JVI.01286-14>
- Powell, L.A., J.M. Fox, N. Kose, A.S. Kim, M. Majedi, R. Bombardi, R.H. Carnahan, J.C. Slaughter, T.E. Morrison, M.S. Diamond, and J.E. Crowe Jr. 2020. Human monoclonal antibodies against Ross River virus target epitopes within the E2 protein and protect against disease. *PLoS Pathog.* 16:e1008517. <https://doi.org/10.1371/journal.ppat.1008517>
- Punjani, A., J.L. Rubinstein, D.J. Fleet, and M.A. Brubaker. 2017. cryoSPARC: algorithms for rapid unsupervised cryo-EM structure determination. *Nat. Methods.* 14:290–296. <https://doi.org/10.1038/nmeth.4169>
- Quiroz, J.A., R.J. Malonis, L.B. Thackray, C.A. Cohen, J. Pallesen, R.K. Jangra, R.S. Brown, D. Hofmann, F.W. Holsberg, S. Shulenin, et al. 2019. Human monoclonal antibodies against chikungunya virus target multiple distinct epitopes in the E1 and E2 glycoproteins. *PLoS Pathog.* 15: e1008061. <https://doi.org/10.1371/journal.ppat.1008061>
- Reed, D.S., D. Xhillari, A.L. Weiss, and R.J. Jaeger. 2016. Chapter 13 aerosol exposure to pathogenic bacteria and virus particles: Standard operating procedure. In *Aerobiology: The toxicology of airborne pathogens and toxins*. The Royal Society of Chemistry. 445–459.
- Roehrig, J.T., J.W. Day, and R.M. Kinney. 1982. Antigenic analysis of the surface glycoproteins of a Venezuelan equine encephalomyelitis virus (TC-83) using monoclonal antibodies. *Virology.* 118:269–278. [https://doi.org/10.1016/0042-6822\(82\)90346-4](https://doi.org/10.1016/0042-6822(82)90346-4)
- Roehrig, J.T., A.R. Hunt, R.M. Kinney, and J.H. Mathews. 1988. In vitro mechanisms of monoclonal antibody neutralization of alphaviruses. *Virology.* 165:66–73. [https://doi.org/10.1016/0042-6822\(88\)90659-9](https://doi.org/10.1016/0042-6822(88)90659-9)
- Roehrig, J.T., and J.H. Mathews. 1985. The neutralization site on the E2 glycoprotein of Venezuelan equine encephalomyelitis (TC-83) virus is composed of multiple conformationally stable epitopes. *Virology.* 142: 347–356. [https://doi.org/10.1016/0042-6822\(85\)90343-5](https://doi.org/10.1016/0042-6822(85)90343-5)
- Ronca, S.E., K.T. Dineley, and S. Paessler. 2016. Neurological sequelae resulting from encephalitic alphavirus infection. *Front. Microbiol.* 7:959. <https://doi.org/10.3389/fmicb.2016.00959>
- Rusnak, J.M., L.C. Dupuy, N.A. Niemuth, A.M. Glenn, and L.A. Ward. 2018. Comparison of aerosol- and percutaneous-acquired Venezuelan equine encephalitis in humans and nonhuman primates for suitability in predicting clinical efficacy under the animal rule. *Comp. Med.* 68: 380–395. <https://doi.org/10.30802/AALAS-CM-18-000027>
- Sabo, M.C., V.C. Luca, J. Prentoe, S.E. Hopcraft, K.J. Blight, M. Yi, S.M. Lemon, J.K. Ball, J. Bukh, M.J. Evans, et al. 2011. Neutralizing monoclonal antibodies against hepatitis C virus E2 protein bind discontinuous epitopes and inhibit infection at a postattachment step. *J. Virol.* 85(14): 7005–7019. <https://doi.org/10.1128/JVI.00586-11>
- Scheres, S.H.W. 2012. RELION: Implementation of a bayesian approach to cryo-EM structure determination. *J. Struct. Biol.* 180:519–530. <https://doi.org/10.1016/j.jsb.2012.09.006>
- Sharma, A., and B. Knollmann-Ritschel. 2019. Current understanding of the molecular basis of Venezuelan equine encephalitis virus pathogenesis and vaccine development. *Viruses.* 11:164. <https://doi.org/10.3390/v11020164>
- Sidwell, R.W., and D.F. Smee. 2003. Viruses of the Bunya- and Togaviridae families: Potential as bioterrorism agents and means of control. *Antivir. Res.* 57:101–111. [https://doi.org/10.1016/s0166-3542\(02\)00203-6](https://doi.org/10.1016/s0166-3542(02)00203-6)
- Silva, L.A., S. Khomandiak, A.W. Ashbrook, R. Weller, M.T. Heise, T.E. Morrison, and T.S. Dermody. 2014. A single-amino-acid polymorphism in chikungunya virus e2 glycoprotein influences glycosaminoglycan utilization. *J. Virol.* 88:2385–2397. <https://doi.org/10.1128/JVI.03116-13>
- Smith, S.A., and J.E. Crowe Jr. 2015. Use of human hybridoma technology to isolate human monoclonal antibodies. *Microbiol. Spectr.* 3:0027–2014. <https://doi.org/10.1128/microbiolspec.AID-0027-2014>
- Smith, S. A., L.A. Silva, J.M. Fox, A.I. Flyak, Flyak, N. Kose, G. Sapparapu, S. Khomandiak, A.W. Ashbrook, K.M. Kahle, et al. 2015. Isolation and characterization of broad and ultrapotent human monoclonal antibodies with therapeutic activity against chikungunya virus. *Cell Host Microbe.* 18:86–95. <https://doi.org/10.1016/j.chom.2015.06.009>
- Smith, T.J., R.H. Cheng, N.H. Olson, P. Peterson, E. Chase, R.J. Kuhn, and T.S. Baker. 1995. Putative receptor binding sites on alphaviruses as visualized by cryoelectron microscopy. *Proc. Natl. Acad. Sci. USA.* 92: 10648–10652. <https://doi.org/10.1073/pnas.92.23.10648>
- Strauss, J.H., and E.G. Strauss. 1994. The alphaviruses: Gene expression, replication, and evolution. *Microbiol. Rev.* 58:491–562. <https://doi.org/10.1128/mr.58.3.491-562.1994>
- Sun, C., C.L. Gardner, A.M. Watson, K.D. Ryman, and W.B. Klimstra. 2014. Stable, high-level expression of reporter proteins from improved alphavirus expression vectors to track replication and dissemination during encephalitic and arthritogenic disease. *J. Virology.* 88:2035–2046. <https://doi.org/10.1128/jvi.02990-13>
- Thompson, B.S., B. Moesker, J.M. Smit, J. Wilschut, M.S. Diamond, and D.H. Fremont. 2009. A therapeutic antibody against west nile virus neutralizes infection by blocking fusion within endosomes. *PLoS Pathog.* 5: e1000453. <https://doi.org/10.1371/journal.ppat.1000453>
- Vanblargan, L.A., J.M. Errico, N.M. Kafai, K.E. Burgomaster, P.N. Jethva, R.M. Broeckel, K. Meade-White, C.A. Nelson, S. Himansu, D. Wang, et al. 2021. Broadly neutralizing monoclonal antibodies protect against multiple tick-borne flaviviruses. *J. Exp. Med.* 218:e20210174. <https://doi.org/10.1084/jem.20210174>
- Voss, J.E., M.-C. Vaney, S. Duquerroy, C. Vonnrhein, C. Girard-Blanc, E. Crublet, A. Thompson, G. Bricogne, and F.A. Rey. 2010. Glycoprotein organization of Chikungunya virus particles revealed by X-ray crystallography. *Nature.* 468:709–712. <https://doi.org/10.1038/nature09555>
- Wang, J., M. Bardelli, D.A. Espinosa, M. Pedotti, T.-S. Ng, S. Bianchi, L. Simonelli, E.X.Y. Lim, M. Foglierini, F. Zatta, et al. 2017. A human B-specific antibody against Zika virus with high therapeutic potential. *Cell.* 171:229–241.e15. <https://doi.org/10.1016/j.cell.2017.09.002>
- Weaver, S.C., R. Winegar, I.D. Manger, and N.L. Forrester. 2012. Alphaviruses: Population genetics and determinants of emergence. *Antivir. Res.* 94:242–257. <https://doi.org/10.1016/j.antiviral.2012.04.002>



- Weger-Lucarelli, J., M.T. Aliota, N. Wlodarchak, A. Kamlangdee, R. Swanson, and J.E. Osorio. 2015. Dissecting the role of E2 protein domains in alphavirus pathogenicity. *J. Virol.* 90:2418–2433. <https://doi.org/10.1128/JVI.02792-15>
- Williamson, L.E., T. Gilliland Jr., P.K. Yadav, E. Binshtein, R. Bombardi, N. Kose, R.S. Nargi, R.E. Sutton, C.L. Durie, E. Armstrong, et al. 2020. Human antibodies protect against aerosolized eastern equine encephalitis virus infection. *Cell.* 183:1884–1900.e23. <https://doi.org/10.1016/j.cell.2020.11.011>
- Williamson, L.E., K.M. Reeder, K. Bailey, M.H. Tran, V. Roy, M.E. Fouch, N. Kose, A. Trivette, R.S. Nargi, E.S. Winkler, et al. 2021. Therapeutic alphavirus cross-reactive E1 human antibodies inhibit viral egress. *Cell.* 184:4430–4446.e22. <https://doi.org/10.1016/j.cell.2021.07.033>
- Young, N.A., and K.M. Johnson. 1969. Antigenic variants of Venezuelan equine encephalitis virus: Their geographic distribution and epidemiologic significance. *Am. J. Epidemiol.* 89:286–307. <https://doi.org/10.1093/oxfordjournals.aje.a120942>
- Yu, X., P.A. McGraw, F.S. House, and J.E. Crowe. 2008. An optimized electroporation-based protocol for generating virus-specific human monoclonal antibodies. *J. Immunol. Methods.* 336:142–151. <https://doi.org/10.1016/j.jim.2008.04.008>
- Zacks, M.A., and S. Paessler. 2010. Encephalitic alphaviruses. *Vet. Microbiol.* 140:281–286. <https://doi.org/10.1016/j.vetmic.2009.08.023>
- Zhang, K. 2016. Gctf: Real-time CTF determination and correction. *J. Struct. Biol.* 193:1–12. <https://doi.org/10.1016/j.jsb.2015.11.003>
- Zhang, R., C.F. Hryc, Y. Cong, X. Liu, J. Jakana, R. Gorchakov, M.L. Baker, S.C. Weaver, and W. Chiu. 2011. 4.4 Å cryo-EM structure of an enveloped alphavirus Venezuelan equine encephalitis virus. *EMBO J.* 30: 3854–3863. <https://doi.org/10.1038/emboj.2011.261>
- Zhang, R., A.S. Kim, J.M. Fox, S. Nair, K. Basore, W.B. Klimstra, R. Rimkunas, R.H. Fong, H. Lin, S. Poddar, et al. 2018. Mxra8 is a receptor for multiple arthritogenic alphaviruses. *Nature.* 557:570–574. <https://doi.org/10.1038/s41586-018-0121-3>
- Zheng, G.X.Y., J.M. Terry, P. Belgrader, P. Ryvkin, Z.W. Bent, R. Wilson, S.B. Ziraldo, T.D. Wheeler, G.P. Mcdermott, J. Zhu, et al. 2017. Massively parallel digital transcriptional profiling of single cells. *Nat. Commun.* 8: 14049. <https://doi.org/10.1038/ncomms14049>
- Zhou, Q.F., J.M. Fox, J.T. Earnest, T.-S. Ng, A.S. Kim, G. Fibriansah, V.A. Kostyuchenko, J. Shi, B. Shu, M.S. Diamond, and S.-M. Lok. 2020. Structural basis of Chikungunya virus inhibition by monoclonal antibodies. *Proc. Natl. Acad. Sci. USA.* 117:27637–27645. <https://doi.org/10.1073/pnas.2008051117>

## Supplemental material

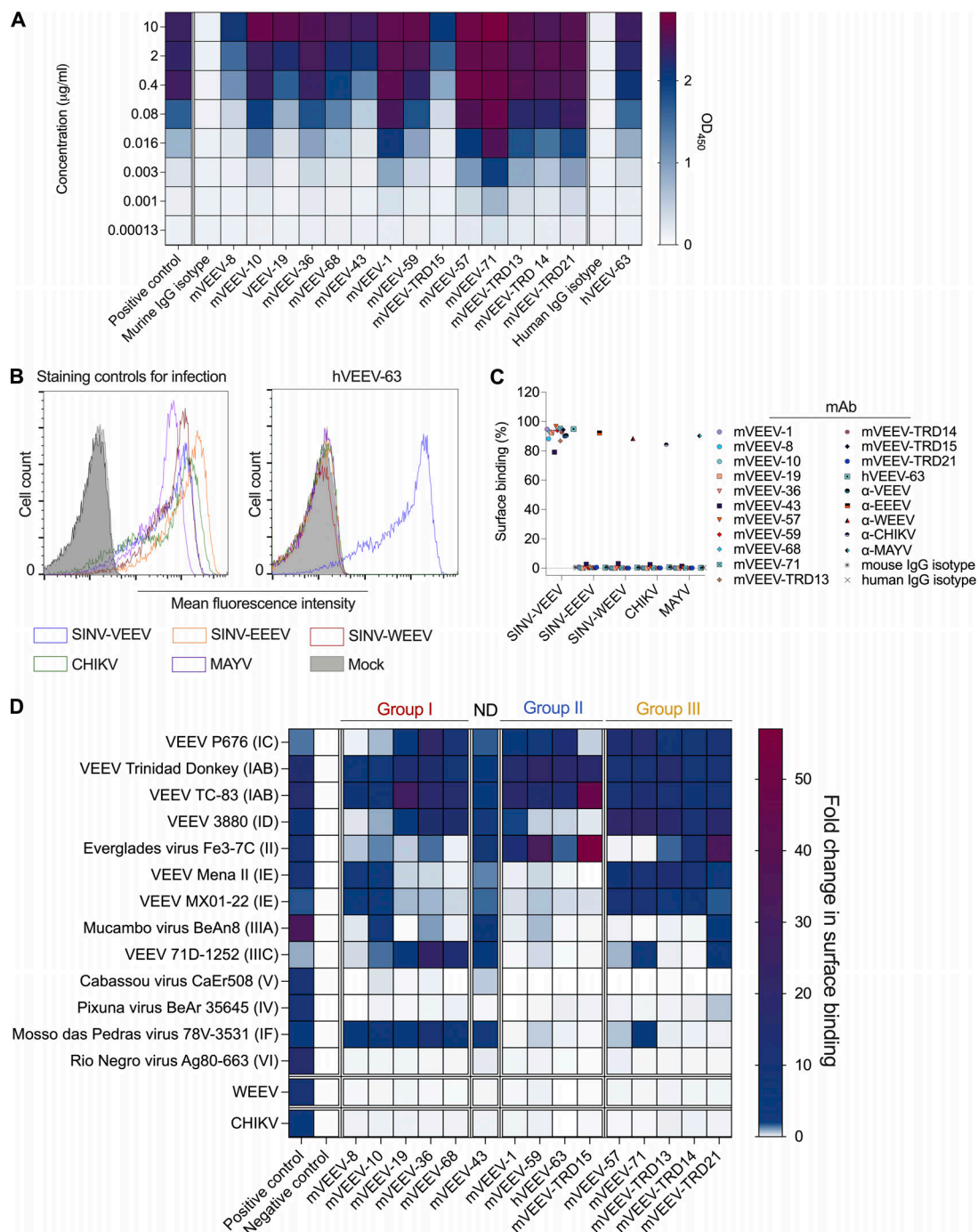


Figure S1. **Cross-reactivity of anti-VEEV mAbs.** (A) Heatmap of anti-VEEV mAbs binding to recombinant VEEV TC-83 E2 ectodomain (E2 residues 1–341) by ELISA. mAb dilutions are 1:5 down each row, beginning with 10  $\mu\text{g/ml}$ . Data represents mean OD<sub>450</sub> units of two experiments performed in duplicate. Murine IgG1 isotype mAb (H77.39; [Sabo et al., 2011](#)); positive control murine anti-VEEV E2 mAb (3B4C-4; [Hunt and Roehrig, 1985](#)). (B and C) Vero cells were inoculated with SINV-VEEV (strain TrD), SINV-EEEV (FL93-939), SINV-WEEV (McMillan), CHIKV (181/25), and MAYV (BeH307) for 24 h and stained for surface viral antigen expression with the panel of new anti-VEEV mAbs, positive controls murine anti-VEEV (3B4C-4), anti-WEEV (WEEV-235), anti-CHIKV (CHK-152; [Pal et al., 2013](#)), anti-MAYV (MAYV-131; [Earnest et al., 2019](#)), or isotype control mAbs. Murine IgG1 isotype (H77.39); human IgG1 isotype (WNV hE16; [Oliphant et al., 2005](#)). Cells were analyzed by flow cytometry. Data are an average of three independent experiments. (B) Representative flow cytometry plot showing alphavirus-infected Vero cells stained with virus-specific mAb (left) or human anti-VEEV mAb hVEEV-63 (right). (C) Surface binding of anti-VEEV and controls anti-alphavirus mAbs to alphavirus-infected cells relative to staining with an isotype mAb. (D) Heatmap of fold-change for mAb binding to different antigenic complex members corresponding to the structural proteins of VEE complex subtypes (virus, strain [subtype]), WEEV (McMillan), or CHIKV (181/25). The relative fold-change for mAb binding was calculated after subtraction of background binding to Expi293F cells and normalized relative to a negative control human mAb (rDENV-2D22; [Fibriansah et al., 2015](#)). Positive control mAbs were used to detect VEEV (1A3B-7; [Roehrig and Mathews, 1985](#)), WEEV (2A3D-5; [Hunt and Roehrig, 1985](#)), and CHIKV (mouse ascites fluid; ATCC). The heatmap corresponds to strength of binding, with transition of color from blue to maroon indicating an increase in fold-change of surface binding. White color indicates no reactivity. mAbs are colored by competition groups as determined in [Fig. 1 A](#). Data represent median values from two experiments performed in technical triplicate.



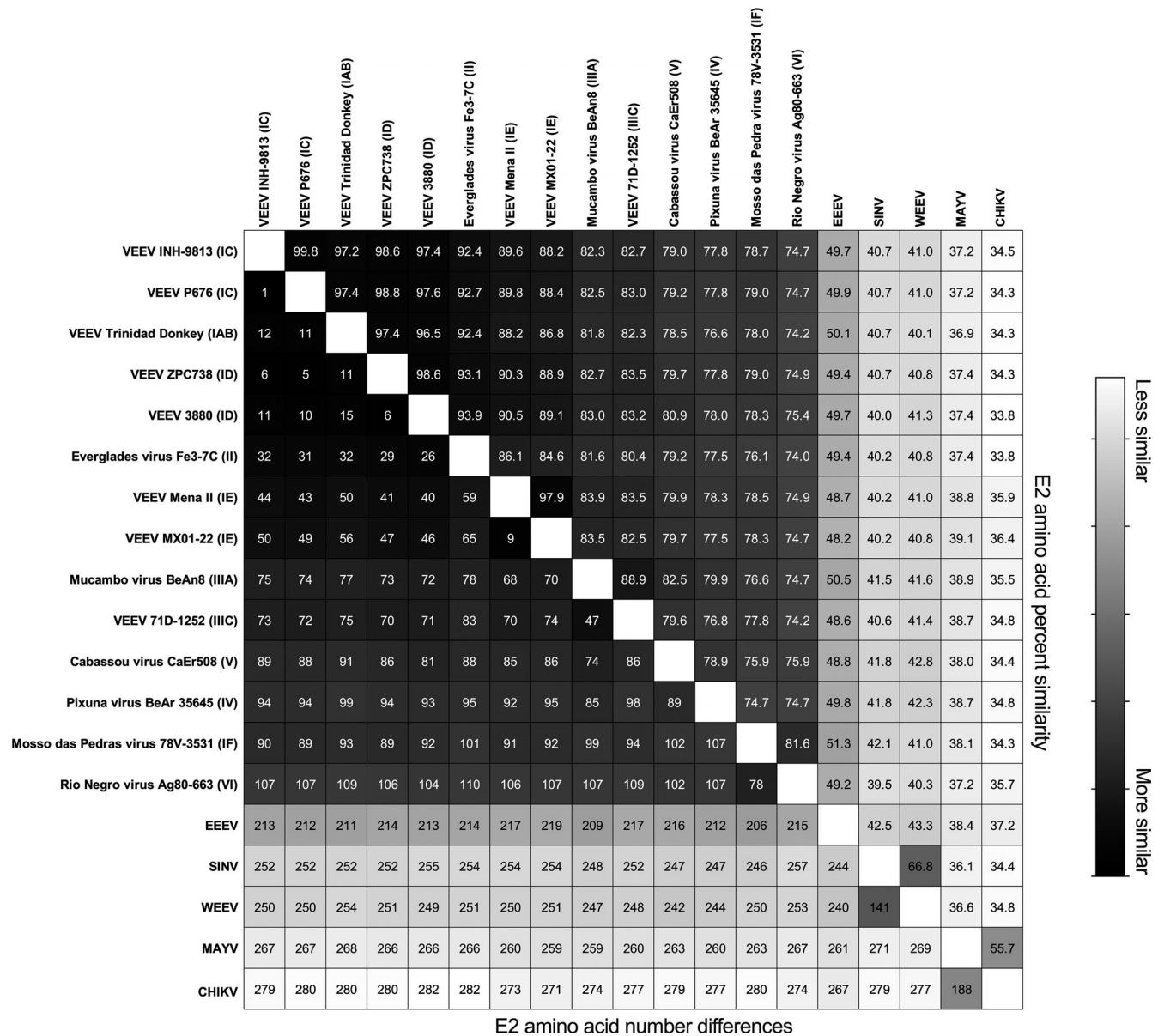
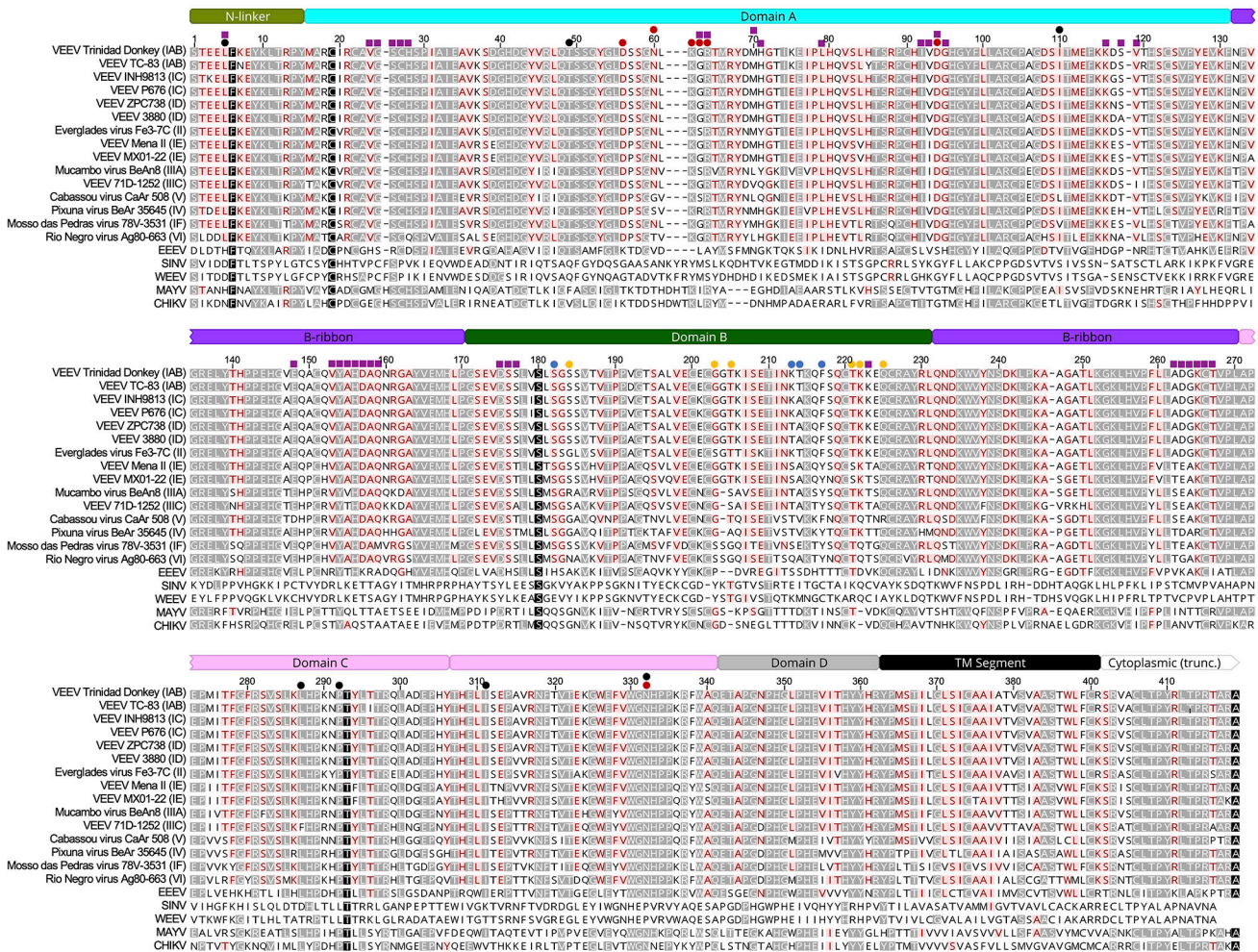


Figure S2. **Alphavirus E2 glycoprotein sequence identity.** The amino acid sequences of E2 glycoproteins for VEE antigenic complex subtypes, EEEV, SINV, WEEV, MAYV, and CHIKV indicated in Fig. 1 B were aligned using Geneious Prime MUSCLE Alignment, set to compute eight iterations, to determine percent identity (top half) and the number of amino acid differences (bottom half). Darker shading indicates increased sequence identity.



**Figure S3. Alphavirus E2 glycoprotein sequence alignment.** The E2 glycoprotein amino acid protein sequence (S1-A419) from vaccine strain VEEV TC-83 and VEE antigenic complex subtypes I-VI: VEEV TrD (subtype IAB), VEEV INH9813 (IC), VEEV P676 (IC), VEEV ZPC738 (ID), VEEV 3880 (ID), Everglades virus Fe3-7C (II), VEEV Mena II (IE), VEEV MX01-22 (IE), Mucambo virus BeAn8 (IIIA), VEEV 71D-1252 (IIIC), Cabassou virus CaEr508 (V), Pixuna virus BeAr 35645 (IV), Mosso das Pedra virus 78V-3531 (IF), Rio Negro virus Ag80-663 (VI), and related encephalitic, EEEV 76V-25343, WEEV McMillan, and arthritogenic, SINV, MAYV BeH407, and CHIKV 181/25 alphaviruses were aligned using Geneious Prime. Key binding residues for each mAb (listed in Table 1) are indicated above the E2 alignment by colored circles. Symbol colors match competition groups determined in Fig. 1 A. Purple squares indicate VEEV receptor LDLRAD3 contact sites (Basore et al., 2021; Ma et al., 2021). Conserved sequences are highlighted in black (100% identity), gray (80–99% identity), pink (60–80% identity), or no highlight (<60% identity). Domains in E2 VEEV TrD are referenced as a color-coded ribbon above the sequence alignment.

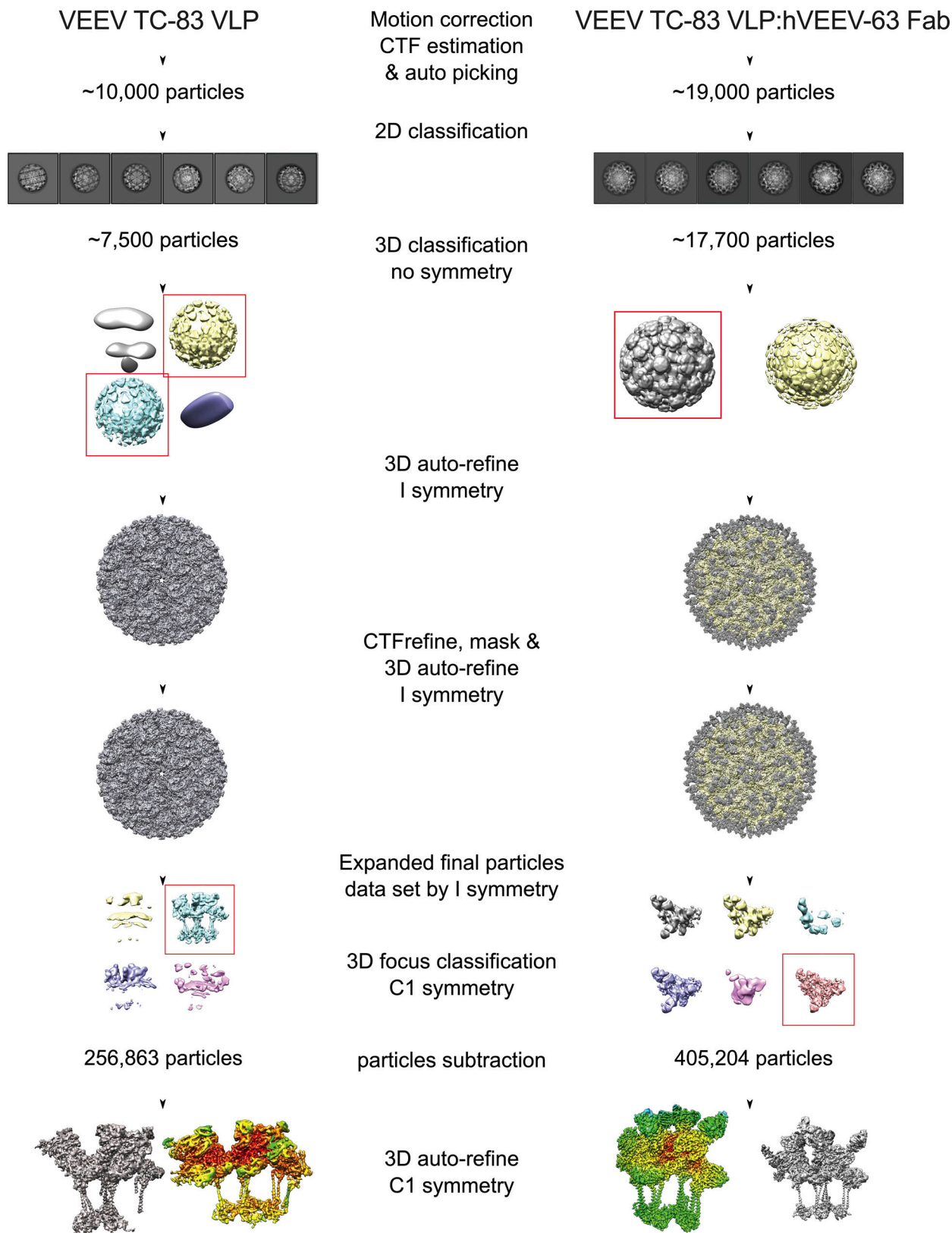


Figure S4. **Cryo-EM processing of the apo-form of VEEV TC-83 VLP or in complex with hVEEV-63 Fab.** Flow chart of cryo-EM processing steps of the maps of VEEV TC-83 VLP and VEEV TC-83 VLP:hVEEV-63 Fab complex.



Provided online are Table S1, Table S2, and Table S3. Table S1 shows comprehensive alanine scanning mutagenesis results for anti-VEEV mAbs and corresponding mutations in the VEEV TrD E2 glycoprotein. Table S2 lists VEEV TrD E2 variants identified in antibody escape mutation pools. Table S3 shows statistical parameters used for high-resolution data collection of VEEV TC-83 VLP and VEEV TC-83 VLP:hVEEV-63 Fab.